



Blastic plasmacytoid dendritic cell neoplasm: genomics mark epigenetic dysregulation as a primary therapeutic target

by Maria Rosaria Sapienza, Francesco Abate, Federica Melle, Stefania Orecchioni, Fabio Fuligni, Maryam Etebari, Valentina Tabanelli, Maria Antonella Laginestra, Alessandro Pileri, Giovanna Motta, Maura Rossi, Claudio Agostinelli, Elena Sabattini, Nicola Pimpinelli, Mauro Truni, Brunangelo Falini, Lorenzo Cerroni, Giovanna Talarico, Rossana Piccioni, Stefano Amente, Valentina Indio, Giuseppe Tarantino, Francesco Brundu, Marco Paulli, Emilio Berti, Fabio Facchetti, Gaetano Ivan Dellino, Francesco Bertolini, Claudio Tripodo, Raul Rabadan, and Stefano A. Pileri

Haematologica 2018 [Epub ahead of print]

Citation: Maria Rosaria Sapienza, Francesco Abate, Federica Melle, Stefania Orecchioni, Fabio Fuligni, Maryam Etebari, Valentina Tabanelli, Maria Antonella Laginestra, Alessandro Pileri, Giovanna Motta, Maura Rossi, Claudio Agostinelli, Elena Sabattini, Nicola Pimpinelli, Mauro Truni, Brunangelo Falini, Lorenzo Cerroni, Giovanna Talarico, Rossana Piccioni, Stefano Amente, Valentina Indio, Giuseppe Tarantino, Francesco Brundu, Marco Paulli, Emilio Berti, Fabio Facchetti, Gaetano Ivan Dellino, Francesco Bertolini, Claudio Tripodo, Raul Rabadan, and Stefano A. Pileri. Blastic plasmacytoid dendritic cell neoplasm: genomics mark epigenetic dysregulation as a primary therapeutic target.

Haematologica. 2018; 103:xxx

doi:10.3324/haematol.2018.202093

Publisher's Disclaimer.

E-publishing ahead of print is increasingly important for the rapid dissemination of science. Haematologica is, therefore, E-publishing PDF files of an early version of manuscripts that have completed a regular peer review and have been accepted for publication. E-publishing of this PDF file has been approved by the authors. After having E-published Ahead of Print, manuscripts will then undergo technical and English editing, typesetting, proof correction and be presented for the authors' final approval; the final version of the manuscript will then appear in print on a regular issue of the journal. All legal disclaimers that apply to the journal also pertain to this production process.

Blastic plasmacytoid dendritic cell neoplasm: genomics mark epigenetic dysregulation as a primary therapeutic target

Maria Rosaria Sapienza^{1*}, Francesco Abate^{2,3*}, Federica Melle⁴, Stefania Orecchioni⁵, Fabio Fuligni⁶, Maryam Etebari¹, Valentina Tabanelli⁴, Maria Antonella Laginestra¹, Alessandro Pileri^{7,8}, Giovanna Motta⁴, Maura Rossi¹, Claudio Agostinelli¹, Elena Sabattini¹, Nicola Pimpinelli⁸, Mauro Truni⁹, Brunangelo Falini¹⁰, Lorenzo Cerroni¹¹, Giovanna Talarico⁵, Rossana Piccioni¹², Stefano Amente¹³, Valentina Indio¹⁴, Giuseppe Tarantino¹⁴, Francesco Brundu², Marco Paulli¹⁵, Emilio Berti¹⁶, Fabio Facchetti¹⁷, Gaetano Ivan Dellino^{12,18}, Francesco Bertolini⁵, Claudio Tripodo^{19*}, Raul Rabadan^{2,3*} and Stefano A. Pileri^{4□*}

Authors' affiliation:

1 Hematopathology Unit, Department of Experimental, Diagnostic, and Specialty Medicine, S. Orsola-Malpighi Hospital, University of Bologna, Bologna, 40138 Italy

2 Department of Systems Biology, Columbia University College of Physicians and Surgeons, New York, New York, 10032 United States of America,

3 Department of Biomedical Informatics, Columbia University College of Physicians and Surgeons, New York, New York, 10032 United States of America

4 Division of Haematopathology, European Institute of Oncology, Milan, 20141 Italy

5 Laboratory of Hematology-Oncology, European Institute of Oncology, Milan, 20141 Italy

6 Department of Genetics and Genome Biology, The Hospital for Sick Children, Toronto, M5G 0A4 Canada

7 Dermatology Unit, Department of Experimental, Diagnostic and Specialty Medicine, University of Bologna, Bologna, 40138 Italy

8 Division Dermatology, Department of Surgery and Translational Medicine, University of Florence, Florence, 50212 Italy

9 Pathological Anatomy Histology & Cytogenetics, Niguarda Cancer Center, Niguarda-Ca' Granda Hospital, Milan, 20162 Italy

10 Institute of Hematology and Center for Hemato-Oncology Research (CREO), University and Hospital of Perugia, Perugia, 06123 Italy

11 Universitätsklinik für Dermatologie und Venerologie, LKH-Univ. Klinikum Graz, Graz, 8036 Austria

12 Department of Experimental Oncology, European Institute of Oncology, Milan, 20141 Italy

13 Department of Molecular Medicine and Medical Biotechnologies, University of Naples 'Federico II', Naples, 80138 Italy

14 "Giorgio Prodi" Cancer Research Center, University of Bologna, Bologna, 40138 Italy.

15 Unit of Anatomic Pathology, Department of Molecular Medicine, University of Pavia and Fondazione IRCCS San Matteo Policlinic, Pavia, 27100 Italy

16 Department of Dermatology, Fondazione IRCCS Ca' Granda - Ospedale Maggiore Policlinic and Milan University, Milan, 20122 Italy

17 Pathology Section, Department of Molecular and Translational Medicine, University of Brescia, Brescia, 2123 Italy

18 Department of Oncology and Hemato-oncology, University of Milan, Milan, 20126 Italy

19 Tumor Immunology Unit, Department of Health Science, Human Pathology Section, University of Palermo School of Medicine, Palermo, 90127 Italy

* Equally contributed.

□ *Alma Mater* Professor, Bologna University

Running Title

Epigenetic matrix and targeted therapy of BPDCN.

Funding

The present work was supported by the AIRC grants IG 15762 and 5x1000 10007 “Genetics-driven targeted management of lymphoid malignancies” and the Grant “Innovative approaches to the diagnosis and pharmacogenetic-based therapies of primary hepatic tumours, peripheral B and T-cell lymphomas and lymphoblastic leukaemias” Strategic Programme 2010-2012 Regione Emilia Romagna - Università (all to SAP).

Correspondence

Maria Rosaria Sapienza, MS, PhD

Molecular Pathology Laboratory,

Hematopathology Unit, Department of Experimental, Diagnostic, and Specialty Medicine, S.

Orsola-Malpighi Hospital, Bologna University Medical School

Via Massarenti, 9 - 40138 Bologna, Italy.

Phone: +39-051-2143047

e-mail: mariarosaria.sapienza@gmail.com

Stefano A. Pileri, MD, *Alma Mater* Professor of Pathology

Division of Haematopathology, European Institute of Oncology

Via Ripamonti, 435 – 20141 Milan, Italy

Phone: +39-02-57489251

e-mail: stefano.pileri@ieo.it; stefano.pileri@unibo.it

Abstract word count: 205

Manuscript word count: 3370

Figures: 3

Tables: None

Supplementary file: 1

Acknowledgments

The authors would like to thank Dr. Clelia Peano, Dr. Simona Righi, Dr. Anna Gazzola and Dr. Claudia Mannu for their technical support and Dr T Maeda (Nagasaki University, Japan) for kindly providing us with the BPDCN cell line CAL-1.

Disclosure of Conflicts of interests

The authors declare that they have no competing interests.

Abstract

Blastic Plasmacytoid Dendritic Cell Neoplasm is a rare and aggressive hematological malignancy currently lacking an effective therapy. To possibly identify genetic alterations useful for a new treatment design, we analyzed by whole-exome sequencing fourteen Blastic Plasmacytoid Dendritic Cell Neoplasm patients and the patient-derived CAL-1 cell line. The functional enrichment analysis of mutational data reported the epigenetic regulatory program as the most significantly undermined ($P < .0001$). In particular, twenty-five epigenetic-modifiers were found mutated (e.g., *ASXL1*, *TET2*, *SUZ12*, *ARID1A*, *PHF2*, *CHD8*); *ASXL1* was the most frequently affected (28.6% of cases). To evaluate the impact of the identified epigenetic mutations at the gene-expression and Histone H3 lysine 27 trimethylation/acetylation levels, we performed additional RNA and Pathology tissue-chromatin immunoprecipitation sequencing experiments; the patients displayed enrichment in gene-signatures regulated by methylation and modifiable by Decitabine administration, shared common H3K27-acetylated regions and featured a set of cell-cycle genes aberrantly up-regulated and marked by promoter acetylation. Collectively, the integration of sequencing data showed the potential of a therapy based on epigenetic agents. Through the adoption of a preclinical Blastic Plasmacytoid Dendritic Cell Neoplasm mouse model, established by the CAL-1 cell line xenografting, we demonstrated the efficacy of the combination of the epigenetic drugs 5'-Azacytidine and Decitabine in controlling the disease progression *in vivo*.

Keywords: BPDCN, 5'-Azacytidine, Decitabine, whole-exome sequencing

Introduction

Blastic Plasmacytoid Dendritic Cell Neoplasm (BPDCN) is a rare malignancy, deriving from precursors of plasmacytoid dendritic cells.¹⁻⁴ It has no clear-cut racial or ethnic predisposition and more often affects elderly males (M/F=3.3:1; mean/median age at diagnosis: 61-67 years). Despite BPDCN patients usually respond to first-line chemotherapy, they almost invariably relapse and display a dismal prognosis with a median overall survival (OS) ranging from 10 to 19 months.² No standardized therapeutic approach has been so far established for BPDCN, even if hematopoietic stem cell transplantation has been shown to achieve remission in selected patients.⁵⁻⁶ Therefore, the development of effective treatments still represents an unmet need.⁷ The pathobiology of BPDCN is poorly understood and the number of reports exploring its molecular features is still limited.⁸⁻²¹ In the last few years, recent advances in the understanding of BPDCN molecular landscape paved the way for novel treatment approaches based on the inhibition of the BCL2 protein²², the activation of the cholesterol efflux²³, the repression of the Bromodomain-containing protein 4 (BRD4)²⁴, and the binding to the interleukin-3 receptor (IL3R).²⁵ All these potential therapeutic options, which are worth being further evaluated, mainly emerge from the analysis of the BPDCN transcriptome or from its antigenic repertoire. The genomic landscape of BPDCN has been less investigated, only few studies having explored the mutational events occurring in BPDCN, mainly through targeted sequencing approaches^{14,16,19,20} and without offering novel prospects on treatment options. In this study, we sequenced the whole-exome (WES) of 14 BPDCN samples and of the BPDCN-derived CAL-1 cell line, to discover specific BPDCN genetic vulnerabilities supporting the design of new therapeutic strategies. The WES mutational findings were complemented by copy number variant (CNV) analysis, RNA and Pathology tissue-chromatin immunoprecipitation (PAT-ChIP) sequencing results. The integration of data allowed us to identify a successful combinatorial therapy based on epigenetic drugs able to control the disease progression in a rapidly progressive BPDCN xenograft model.

Methods

BPDCN samples

We collected 14 BPDCN cryopreserved cutaneous biopsies at diagnosis, 9 matched saliva samples and the BPDCN patient-derived cell line, CAL-1. The pathological cases were evaluated as previously described¹⁷ and diagnosed by experienced haematopathologists (CA, EB, FF, LC, MP, ES, CT, MT, and SAP) according to the WHO diagnostic criteria classification.² Informed consent was obtained from each patient in accordance with the Ethical Review Board of the Department of Experimental, Diagnostic, and Specialty Medicine of the University of Bologna and the Declaration of Helsinki. The DNA was extracted as reported in the Online Supplementary Appendix. The main clinical, immunohistochemical and cytogenetic features of BPDCN patients are shown in Table S1-S2.

Whole-exome Sequencing (WES) analysis

We performed paired-end sequencing of matched tumor/normal DNA samples (9 cases), tumor only DNA samples (5 cases), and the CAL-1 cell line (Table S3) by using the TruSeq Exome Kit and Nextera Rapid Capture Exome kit (Illumina). For more details see the Online Supplementary Appendix.

Sanger Sequencing

We validated by Sanger sequencing two candidate nonsense somatic mutations of *SUZ12* and *ASX1* occurring in two patients, respectively. as described in the Online Supplementary Appendix.

Targeted sequencing

We performed MiSeq targeted sequencing (Illumina) of the 14 BPDCN tumor patients, 7 normal matched saliva samples and the CAL-1 cell line, already analysed by WES. More bioinformatics details are provided in the Online Supplementary Appendix.

RNA sequencing (RNA-seq) analysis

Five BPDCN cases studied by WES and targeted sequencing had enough material for RNA extraction and sequencing: these samples represented the RNA-seq discovery set. We also collected additional 4 BPDCN cryopreserved cutaneous biopsies, sufficient only for RNA sequencing experiments, used as RNA-seq extension set. RNA of 4 normal plasmacytoid dendritic cell (pDCs) samples was purchased from AllCells (Alameda, CA, US) and used for comparison. For details, see Table S10 and Online Supplementary Appendix

Pathology tissue-chromatin immunoprecipitation (PAT-ChIP) sequencing

The BPDCN_25 and BPDCN_37 patients were provided with one skin biopsy: half cryopreserved and used for WES, targeted and RNA sequencing analysis and half fixed in formalin, included in paraffin and used for PAT-ChIP sequencing analysis. PAT-ChIP experiments were performed as in Fanelli *et al.*²⁶ For more details see the Online Supplementary Appendix.

CAL-1 cell line

CAL-1, a BPDCN cell line²⁷, was cultured as reported¹⁸. The CAL-1 gene expression profile of a previous study was used¹⁷

(<http://www.ncbi.nlm.nih.gov/geo/query/acc.cgi?acc=GSE62014>)

Mouse model and *in vivo* treatments

Experiments were carried out on nonobese diabetic severe combined immunodeficient NOD/SCID interleukin-2 receptor γ (IL-2R γ)-null (NSG) mice, 6 to 8 weeks old as previously reported.¹³ All animal experiments were carried out in accordance with the applicable Italian laws (D.L.vo 26/14 and following amendments) and the institutional guidelines. All *in vivo* studies were ratified by the Italian Ministry of Health. For induction of BPDCN in mice, 5.000 CAL-1 cells were injected intravenously (i.v.) through the lateral tail vein in non-irradiated mice. Engrafted mice were then treated with Bortezomib, 5'-Azacytidine, Decitabine and Romidepsin as detailed in the Online Supplementary Appendix.

Results

Whole-exome sequencing reveals the epigenetic program dysregulation as the main theme of BPDCN mutational landscape

We collected 14 BPDCN cases with a mean age of 56 years at diagnosis (range 9-89 years), a male-to-female ratio of 10:4 and the classical BPDCN presentation (Table S1-S2).¹

The enrolled patients underwent different treatment regimens and 78.5 % (11/14) died of the disease from 6.3 to 76 months after the diagnosis or were lost at follow-up. Most patients who underwent autologous and/or allogenic hematopoietic stem cell transplantation experienced a prolonged survival.

We performed whole exome sequencing (WES) on 14 BPDCN cases, and on BPDCN patient-derived CAL-1 cell line and identified 1,302 nonsynonymous SNVs represented predominantly by missense SNVs (n =1,251), nonsense SNVs (n = 47) and frameshift insertions/deletions (n = 7) (Table S3). To verify the robustness of the WES analysis, 2 randomly-selected variants occurring in *ASXL1* and *SUZ12* genes, respectively, were validated by Sanger sequencing (Figure S1). To extend the validation to a higher number of samples and mutations, a targeted sequencing approach was adopted: 21 SNVs were interrogated by MiSeq Illumina technology in the same BPDCN cases analyzed by WES and a concordance of 95.2% (20/21 SNVs) was achieved, underlining a high consistency of data, as reported in the supplementary data (Table S4-S6). The 1,302 nonsynonymous SNVs detected by WES affected 1,166 genes, all but 7 known to be related with pathological conditions and reported as mutated in the Catalogue of Somatic Mutations in Cancer (COSMIC_v66).

To identify the biological processes prominently altered by the mutational events, we performed a functional enrichment analysis of the 9 genes that were recurrently mutated (≥ 3 samples) and the 45 genes impacted by deleterious - nonsense or frameshift - SNVs. Among the top 10 significantly enriched biological processes, the epigenetic program resulted the most represented ($P = .0001$), followed by the hematopoietic stem cell homeostasis, the Rac signaling and the gamma-aminobutyric acid (GABA) secretion (Figure 1A, Table S7). The *ASXL1* gene, proved to be the most frequently mutated (28%, 4/14 samples), followed by *TET2* (21%, 3/14 samples) and, both genes displayed in prevalence nonsense or frameshift

SNVs located within or upstream of the catalytic domain of the proteins, potentially leading to their functional disruption (Figure 1B, Table S8). To identify among the 1,166 BPDCN mutated genes those implicated into the epigenetic regulation, we interrogated the Gene Ontology database²⁸ and found 25 mutated epigenetic modifier genes controlling chromatin accessibility (*ARID1a*, *CHD8*, *SMARCA1*), DNA methylation (*TET2*, *IDH2*), or histone post-transcriptional modifications [methylation (*ASXL1*, *SUZ12*, *MLL* family), demethylation (*KDM4D*), acetylation (*EP300*, *EP400*), ubiquitination (*PHC1*, *PHC2*), dephosphorilation (*EYA2*), and exchange (*SRCAP*)]. Of note, 12/14 (86%) BPDCN samples harbored at least one of the 25 epigenetic regulator genes mutated and specifically 8/14 (57,14%) patients presented a deleterious lesion (nonsense/frameshift SNV) (Figure 1C and Table S9). Many SNVs clustered in the histone methylation pathway, specifically, in genes belonging to the Polycomb-repressive complex 2 (*ASXL1*, *ASXL3*, *SUZ12*) and in histone methyltransferases (*ASH1L1*, *SETMAR*, *MLL*), possibly mining the integrity of the methylation program. Besides genetic lesions targeting epigenetic regulators, we also detected mutations potentially affecting molecular programs commonly deregulated in myeloid malignancies such as the RAS signaling²⁹ (hot-spot SNVs on *KRAS* or *NRAS*, alternatively), the DNA repair/cycle progression³⁰ (SNVs on *BRCA1*, *ATM*, *ATR*, and *RAD52*), the Wnt-signaling³¹ (SNVs on *WNT3*, *WNT7B*, *WNT10* and *BCL9L*), the cell growth³² (SNVs on *RUNX2*, *MAPK1*), and the splicing machinery³³ (a SNV on *ZRSR2*) (Figure 1C).

WES data was also used for cytogenetic copy number variants (CNVs) analysis, which highlighted extensive losses along the chromosome 9 and the associated deletion of the tumor suppressor *CDKN2A* gene in 8/14 (57%) BPDCN samples (Figure S2 and Table S2), as already reported in the literature.^{12,15,20} In addition, CNV analysis showed that deletions affected six of the nine genes recurrently mutated; deletions were always mutually exclusive with mutations (Figure S3). However, no significant correlation was found between genetic lesions and clinical data.

BPDCN Transcriptome profiling confirms the dysregulation of epigenetic programs

Genetic lesions in key epigenetic modifier genes and in related regulatory networks can induce profound perturbations in the transcriptional homeostasis of the cell. To further substantiate the impact of mutations affecting the chromatin remodeling pathway in BPDCN, we performed RNA sequencing of 5 BPDCNs, considered as the discovery set, already studied by WES and MiSeq targeted sequencing (Table S10). We analyzed the patients transcriptomes in comparison with that of 4 normal plasmacytoid dendritic cell (pDC) samples isolated from the peripheral blood of healthy individuals and used as controls. BPDCN tumor samples and pDCs segregated separately, according to their gene expression profiles (Figure 2A). Two thousand and thirty-four genes (2,034) were significantly deregulated among patients, and about half of them was upregulated (46%) in the BPDCN setting. Gene set enrichment analysis (GSEA) reported the significant deregulation of two genetic signatures, involved in the methylation process, driven by *KDM5B*³⁴ histone demethylase and *PRMT5*³⁵ methyltransferase-associated gene, respectively. Of note, GSEA also detected the significant enrichment of a set of genes associated with the response to a DNA demethylating agent³⁶, namely Decitabine (Figure 2B) The GSEA results (NES ≥ 2 ; FDR q-value $\leq .0001$) were then validated in an extension set of 4 BPDCN samples and in CAL-1 cell line (Figures S4-S5).

Genome-wide ChIP-sequencing substantiates epigenetic dysregulation of cell cycle program in BPDCN

To investigate if the transcriptional deregulation of BPDCNs could be linked to specific epigenetic assets, we analysed the histone acetylation/methylation profiles of two selected BPDCN patients (BPDCN_25 and BPDCN_37). The trimethylation at lysine 27 of histone 3 (H3K27me3) is closely associated with inactive gene promoters, while its acetylation (H3K27ac) well correlates with gene activation, the two epigenetic modifications being mutually exclusive. On this premise, we analysed the genome-wide distribution of trimethylation and acetylation profiles of H3K27 in BPDCN cases. The analysis of PAT-ChIP sequencing data demonstrated that the two patients converged on the same pattern of histone acetylation, sharing as much as the 43,6% of the acetylated promoters (Figures 2C-D). PAT-ChIP sequencing results were then integrated with the RNA sequencing data leading to

identify of a signature of 86 genes marked by promoter acetylation and significantly overexpressed in the BPDCN RNA sequencing sets. Gene Ontology analysis of the 86 selected genes highlighted the enrichment in biological processes involved in cell cycle progression (*FDR q-value* <.001, Figure 2E, Table S11).

In vivo BPDCN modeling demonstrates combined epigenetic therapy as effective in controlling disease progression.

The integration of results obtained from WES, RNA sequencing and PAT-ChIP-sequencing experiments clearly pointed to a fundamental role of epigenetic dysregulation in BPDCN and allowed us to hypothesize that this malignancy could display susceptibility to drugs active on the epigenetic regulation. Following the demonstration that the CAL-1 cell line shared with primary BPDCN samples mutations clustering in chromatin remodeling pathway (Figure 1C) and enrichment in the same epigenetic programs (Figure S5), we developed an *in vivo* CAL-1 xenograft BPDCN-like model to explore the effects of treatments targeting the acetylation, methylation, and also the NF- κ B pathways - according to previous results.^{17,18} To this end, we focused on four different FDA approved compounds: 5'-Azacytidine, Decitabine, Romidepsin and Bortezomib.

NSG mice intravenously injected with 5×10^3 CAL-1 cells rapidly developed a systemic BPDCN-like progressive disease, which was defined by the flow cytometry identification of human CD56⁺CD38⁺ malignant cells in the peripheral blood, bone marrow, spleen and liver, as evaluated at 39 days of the injection (Figure 3A). The pathological infiltration by malignant BPDCN cells in the mouse model was also confirmed, at the same time point, by the histopathological analysis of the bone marrow and spleen samples, which showed the presence of atypical cells with blastic morphology and expressing the human CD303/BDCA2 pDC marker (Figure 3B). Xenografted mice were divided into 11 treatment groups (n=110 mice) 1 day after CAL-1 injection and treated with either saline or with the hypo-methylating agents 5'-Azacytidine or Decitabine, the proteasome inhibitor Bortezomib, and the histone deacetylases inhibitor Romidepsin, used as single agents or in combination, according to the treatment schedule summarized in Figure 3C. The administration of 5'-Azacytidine and Decitabine used as single agents significantly prolonged the mice overall survival as compared with saline (median survival 43.6 days vs 32 days, *P* < .01 for 5'-Azacytidine; median survival 44.7 days vs 32 days, *P* < .05 for Decitabine) while neither Bortezomib nor Romidepsin alone showed beneficial effects on the disease outcome. When the same agents

were associated in combined treatment experiments, three different combinations proved to significantly prolong mouse survival, namely the association of Romidepsin and Decitabine (median survival 42.8 days vs 32 days, $P < .01$), the combination of Romidepsin, Decitabine, and 5'-Azacytidine (median survival 41.8 days vs 32 days, $P < .05$) and the association of Decitabine and 5'-Azacytidine (median survival 52.8 days vs 32 days, $P < .01$), which achieved the best result in terms of survival (Figure 3D). Consistently, 5'-Azacytidine and Decitabine administered alone reduced the CAL-1-induced splenomegaly as evaluated at day 39 post-injection and their combination proved to be even more effective (Figure 3E).

Discussion

BPDCN is a rare myeloid malignancy with dismal prognosis and no standard therapy. In the present study, we performed whole-exome sequencing (WES) of the largest series of BPDCNs that – to the best of our knowledge - has so far been reported in the literature. Thanks to the integration of WES with RNA and PAT-ChIP sequencing, we provide new insights into BPDCN pathobiology by highlighting the dysregulation of epigenetic program as a hallmark of the disease and suggest possible novel therapeutic interventions.

We found BPDCN patients extensively affected by mutations of genes involved in the epigenetic regulation: 25 epigenetic modifiers were mutated in almost all BPDCN patients (13/14) and the CAL-1 cell line. In more than half patients (8/14), the mutations heralded damaging functional alterations (Figure 1C). Some of the mutated genes have already been reported in previous studies (e.g. *ASXL1*, *RAS*, *ATM*, *ARID1A*, and *IDH2*), although at times at different rates than in our series (see *ASXL1* and *TET2*, which were found to be mutated in 28.6% and 21.4% of our samples vs. 32% and 36% of those of Menezes et al.).¹⁹ On this respect, we wish to underline that the aim of our study was not only to extensively explore the mutational landscape of BPDCN but possibly translate molecular notions into a pre-clinical approach. In any case, thanks to the employment of a whole-exome sequencing approach, which did not limit our investigation to *a priori*-selected genes, we recognized additional mutated epigenetic factors, never described before but potentially relevant in the BPDCN context, like *PHF2* histone demethylase that enhances the TP53-tumor suppressor activity³⁷ and the *CHD8* Chromodomain helicase DNA-binding protein-8 that promotes the E2F-dependent transcription and cell cycle progression.³⁸ Besides the epigenetic pathway, we also detected mutations affecting programs common to other myeloid malignancies, such as the DNA repair process,³⁰ the Wnt/ β -catenin signaling³¹ and the differentiation pathway.³² Importantly, the functional enrichment analysis of whole-exome sequencing data showed that among all genes/pathways explored, the epigenetic program was the most deregulated one ($P < .0001$).

To evaluate the impact of the identified epigenetic mutations at gene expression level we analysed the transcriptome of samples studied by WES. Among up-regulated genes, the gene set enrichment analysis (GSEA) revealed the significant enrichment of two methylation pathways, respectively driven by the *KDM5B* histone-demethylase³⁴ and by the *PRMT5*

arginine methyltransferase-5:³⁵ these two epigenetic modifiers are reported as over-expressed in several cancer types and also represent promising therapeutic targets.³⁹ Blockade of the PRMT5 activity reduces cell survival in chronic myelogenous leukemia⁴⁰ and inhibition of *KDM5B* demethylation correlates with cell growth arrest in hepatocellular carcinoma and breast cancers.^{41,42} We also identified the overexpression of one gene signature³⁶ specifically responsive to the administration of the hypomethylating agent Decitabine: a molecular finding bearing important therapeutic implications ($FDR\ q = 1.85E-5$). To gain a functional insight into the epigenetic landscape of BPDCN samples, we performed PAT-ChIP sequencing of H3K27-acetylation/trimethylation signals of two BPDCN patients. The trimethylation of H3K27 marks inactive gene promoters and enhancers, while its acetylation correlates with gene activation.⁴³ PAT-ChIP sequencing data showed that the two patients converged on the same epigenetic pattern sharing about half of the identified H3K27-acetylated promoters. Interestingly, the common acetylated regions comprised 10 super-enhancers (SE) bound by the Bromodomain-containing protein 4 (BRD4), as described by Ceribelli *et al* in a recent work on BPDCN (data not shown).²⁴

The integration of PAT-ChIP and the RNA sequencing data highlighted a set of 86 genes involved in the cell-cycle progression aberrantly overexpressed and marked by H3K27-promoter acetylation. This finding lets envisage that the cell-cycle deregulation could be driven by H3K27-acetylation signals, a hypothesis deserving future *ad-hoc* studies that can help to clarify the mechanism of proliferation of this largely obscure disease.

The disease rareness (incidence of 0.000045%) and its extremely aggressive behavior (OS from 10 to 19 months) limited the number of available patients included in biological and/or clinical studies. For these reasons, not surprisingly, BPDCN is still an orphan tumor lacking a standardized and effective therapeutic approach. In the last few years, new molecular studies opened the way to innovative target therapies (e.g., Bortezomib^{17,18}, Venetoclax²², BET-inhibitors²⁴, SL-401²⁵), some of which, are showing promising results, and same safety concerns, in early clinical trials. Of note, all the treatments proposed, mainly resulted from the investigation of the RNA transcriptome, while the DNA features of BPDCN patients were scarcely evaluated.

We thus decided to tackle this yet incurable disease by designing the first therapeutic strategy modeled on the DNA mutational status of BPDCN patients, analyzed by whole exome sequencing. The WES mutational findings enhanced by the RNA and PAT-ChIP sequencing results clearly evidenced the prominent role of the epigenetic program dysregulation among BPDCN patients and guided our therapeutic approach towards the use of epigenetic agents.

In particular, we tested *in vivo* the efficacy of FDA-approved epigenetic drugs which could be considered for potential repositioning in clinical trials: two hypomethylating agents such as Decitabine and 5'-Azacytidine, and the histone deacetylase inhibitor Romidepsin. We hypothesized that these drugs could impact on tumor progression as: I) BPDCN patients displayed potential sensitivity to hypomethylating agents, particularly to Decitabine, as detected by GSEA analysis; II) both 5'-Azacytidine and Decitabine are currently in use for the treatment of myelodysplastic syndromes,^{44,45} which are myeloid neoplasms sharing with BPDCN many epigenetic mutated genes; III) preclinical studies on several malignancies demonstrated that the action of Decitabine is synergized by Romidepsin.⁴⁶ In the light of this, our experimental design focused on epigenetic drugs with a large scale activity, aiming to explore whether we might induce cell death by perturbation of the malignant epigenetic programme. In addition to the epigenetic drugs, we also verified the efficacy of Bortezomib, a proteasome inhibitor, which was previously shown to significantly induce *in vitro* and *in vivo* BPDCN cells death^{17,18}. Our experiments revealed that the treatment with 5'-Azacytidine in combination with Decitabine significantly inhibits disease progression and extend survival ($p < 0.01$) in a preclinical mouse model. In the past, two reports experimented the use of 5'-Azacytidine on elderly BPDCN patients, though this therapeutic choice was not yet sustained by a molecular rationale.^{47,48} Here we demonstrated that 5'-Azacytidine is more effective in tumor eradication if combined with Decitabine. Further studies are ongoing to elucidate the synergistic mechanisms between the two drugs.

In conclusion, we identified the deregulation of epigenetic program as a genetic hallmark of BPDCN and suggested a novel therapeutic approach based on the combination of two hypomethylating agents 5'-Azacytidine and Decitabine to be tested in future clinical trials.

References

1. Chaperot L, Bendriss N, Manches O, et al. Identification of a leukemic counterpart of the plasmacytoid dendritic cells. *Blood*. 2001;97(10):3210-3217.
2. Swerdlow SH, Campo E, Hazzis NL, et al. Facchetti F, Jones D, Petrella T. Blastic plasmacytoid dendritic cell neoplasm. In: Swerdlow SH, Campo E, Hazzis NL, et al., eds. *WHO Classification of Tumors of Haematopoietic and Lymphoid Tissues*. Lyon: IARC press; 2008:145-147.
3. Facchetti F, Cigognetti M, Fisogni S, Rossi G, Lonardi S, Vermi W. Neoplasms derived from plasmacytoid dendritic cells. *Mod Pathol*. 2016;29(2):98-111.
4. Garnache-Ottou F, Feuillard J, Ferrand C, et al. Extended diagnostic criteria for plasmacytoid dendritic cell leukaemia. *Br J Haematol*. 2009;145(5):624-636.
5. Pagano L, Valentini CG, Pulsoni A, et al. Blastic plasmacytoid dendritic cell neoplasm with leukemic presentation: an Italian multicenter study. *Haematologica*. 2013;98(2):239-246.
6. Roos-Weil D, Dietrich S, Boumendil A, et al. Stem cell transplantation can provide durable disease control in blastic plasmacytoid dendritic cell neoplasm: a retrospective study from the European Group for Blood and Marrow Transplantation. *Blood*. 2013;121(3):440-446.
7. Pemmaraju N. Blastic plasmacytoid dendritic cell neoplasm. *Clin Adv Hematol Oncol*. 2016;14(4):220-222.

8. Petrella T, Dalac S, Maynadie M, et al. CD4+ CD56+ cutaneous neoplasms: a distinct hematological entity? Groupe Francais d'Etude des Lymphomes Cutanes (GFELC). *Am J Surg Pathol.* 1999;23(2):137-146.
9. Leroux D, Mugneret F, Callanan M, et al. CD4(+), CD56(+) DC2 acute leukemia is characterized by recurrent clonal chromosomal changes affecting 6 major targets: a study of 21 cases by the Groupe Francais de Cytogenetique Hematologique. *Blood.* 2002;99(11):4154-4159.
10. Reichard KK, Burks EJ, Foucar MK, et al. CD4(+) CD56(+) lineage-negative malignancies are rare tumors of plasmacytoid dendritic cells. *Am J Surg Pathol.* 2005;29(10):1274-1283.
11. Dijkman R, van Doorn R, Szuhai K, Willemze R, Vermeer MH, Tensen CP. Gene-expression profiling and array-based CGH classify CD4+CD56+ hematodermic neoplasm and cutaneous myelomonocytic leukemia as distinct disease entities. *Blood.* 2007;109(4):1720-1727.
12. Wiesner T, Obenaus AC, Cota C, Fried I, Speicher MR, Cerroni L. Alterations of the cell-cycle inhibitors p27(KIP1) and p16(INK4a) are frequent in blastic plasmacytoid dendritic cell neoplasms. *J Invest Dermatol.* 2010;130(4):1152-1157.
13. Agliano A, Martin-Padura I, Marighetti P, et al. Therapeutic effect of lenalidomide in a novel xenograft mouse model of human blastic NK cell lymphoma/blastic plasmacytoid dendritic cell neoplasm. *Clin Cancer Res.* 2011;17(19):6163-6173.
14. Jardin F, Ruminy P, Parmentier F, et al. TET2 and TP53 mutations are frequently observed in blastic plasmacytoid dendritic cell neoplasm. *Br J Haematol.* 2011;153(3):413-416.

15. Lucioni M, Novara F, Fiandrino G, et al. Twenty-one cases of blastic plasmacytoid dendritic cell neoplasm: focus on biallelic locus 9p21.3 deletion. *Blood*. 2011;118(17):4591-4594.
16. Alayed K, Patel KP, Konoplev S, et al. TET2 mutations, myelodysplastic features, and a distinct immunoprofile characterize blastic plasmacytoid dendritic cell neoplasm in the bone marrow. *Am J Hematol*. 2013;88(12):1055-1061.
17. Sapienza MR, Fuligni F, Agostinelli C, et al. Molecular profiling of blastic plasmacytoid dendritic cell neoplasm reveals a unique pattern and suggests selective sensitivity to NF- κ B pathway inhibition. *Leukemia*. 2014;28(8):1606-1616.
18. Philippe L, Ceroi A, Bole-Richard E, et al. Bortezomib as a new therapeutic approach for blastic plasmacytoid dendritic cell neoplasm. *Haematologica*. 2017;102(11):1861-1868.
19. Menezes J, Acquadro F, Wiseman M, et al. Exome sequencing reveals novel and recurrent mutations with clinical impact in blastic plasmacytoid dendritic cell neoplasm. *Leukemia*. 2014;28(4):823-829.
20. Stenzinger A, Endris V, Pfarr N, et al. Targeted ultra-deep sequencing reveals recurrent and mutually exclusive mutations of cancer genes in blastic plasmacytoid dendritic cell neoplasm. *Oncotarget*. 2014;5(15):6404-6413.
21. Emadali A, Hoghoughi N, Duley S, et al. Haploinsufficiency for NR3C1, the gene encoding the glucocorticoid receptor, in blastic plasmacytoid dendritic cell neoplasms. *Blood*. 2016;127(24):3040-3053.

22. Montero J, Stephansky J, Cai T, et al. Blastic Plasmacytoid Dendritic Cell Neoplasm Is Dependent on BCL2 and Sensitive to Venetoclax. *Cancer Discov.* 2017;7(2):156-164.
23. Ceroi A, Masson D, Roggy A, et al. LXR agonist treatment of blastic plasmacytoid dendritic cell neoplasm restores cholesterol efflux and triggers apoptosis. *Blood.* 2016;128(23):2694-2707.
24. Ceribelli M, Hou ZE, Kelly PN, et al. A Druggable TCF4- and BRD4-Dependent Transcriptional Network Sustains Malignancy in Blastic Plasmacytoid Dendritic Cell Neoplasm. *Cancer Cell.* 2016;30(5):764-778.
25. Angelot-Delettre F, Roggy A, Frankel AE, et al. In vivo and in vitro sensitivity of blastic plasmacytoid dendritic cell neoplasm to SL-401, an interleukin-3 receptor targeted biologic agent. *Haematologica.* 2015;100(2):223-230.
26. Fanelli M, Amatori S, Barozzi I, et al. Pathology tissue-chromatin immunoprecipitation, coupled with high-throughput sequencing, allows the epigenetic profiling of patient samples. *Proc Natl Acad Sci U S A.* 2010;107(50):21535-21540.
27. Maeda T, Murata K, Fukushima T, et al. A novel plasmacytoid dendritic cell line, CAL-1, established from a patient with blastic natural killer cell lymphoma. *Int J Hematol.* 2005;81(2):148-154.
28. Ashburner M, Ball CA, Blake JA, et al. Gene ontology: tool for the unification of biology. The Gene Ontology Consortium. *Nat Genet.* 2000;25(1):25-29.
29. Ward AF, Braun BS, Shannon KM. Targeting oncogenic Ras signaling in hematologic malignancies. *Blood.* 2012;120(17):3397-3406.

30. Guarini A, Marinelli M, Tavolaro S, et al. ATM gene alterations in chronic lymphocytic leukemia patients induce a distinct gene expression profile and predict disease progression. *Haematologica*. 2012;97(1):47-55.
31. Simon M, Grandage VL, Linch DC, Khwaja A. Constitutive activation of the Wnt/beta-catenin signalling pathway in acute myeloid leukaemia. *Oncogene*. 2005;24(14):2410-2420.
32. Kuo YH, Zaidi SK, Gornostaeva S, Komori T, Stein GS, Castilla LH. Runx2 induces acute myeloid leukemia in cooperation with Cbfbeta-SMMHC in mice. *Blood*. 2009;113(14):3323-3332.
33. Togami K, Madan V, Li J. et al. Blastic Plasmacytoid Dendritic Cell Neoplasm (BPDCN) Harbors Frequent Splicesome Mutations That Cause Aberrant RNA Splicing Affecting Genes Critical in pDC Differentiation and Function. *Blood*. 2016;128(22):738.
34. Scibetta AG, Santangelo S, Coleman J, et al. Functional analysis of the transcription repressor PLU-1/JARID1B. *Mol Cell Biol*. 2007;27(20):7220-7235.
35. Pal S, Vishwanath SN, Erdjument-Bromage H, Tempst P, Sif S. Human SWI/SNF-associated PRMT5 methylates histone H3 arginine 8 and negatively regulates expression of ST7 and NM23 tumor suppressor genes. *Mol Cell Biol*. 2004;24(21):9630-9645.
36. Missiaglia E, Donadelli M, Palmieri M, Crnogorac-Jurcevic T, Scarpa A, Lemoine NR. Growth delay of human pancreatic cancer cells by methylase inhibitor 5-aza-2'-deoxycytidine treatment is associated with activation of the interferon signalling pathway. *Oncogene*. 2005;24(1):199-211.

37. Lee KH, Park JW, Sung HS, et al. PHF2 histone demethylase acts as a tumor suppressor in association with p53 in cancer. *Oncogene*. 2015;34(22):2897-2909.
38. Subtil-Rodriguez A, Vazquez-Chavez E, Ceballos-Chavez M, et al. The chromatin remodeller CHD8 is required for E2F-dependent transcription activation of S-phase genes. *Nucleic Acids Res*. 2014;42(4):2185-2196.
39. Rotili D, Mai A. Targeting Histone Demethylases: A New Avenue for the Fight against Cancer. *Genes Cancer*. 2011;2(6):663-679.
40. Jin Y, Zhou J, Xu F, et al. Targeting methyltransferase PRMT5 eliminates leukemia stem cells in chronic myelogenous leukemia. *J Clin Invest*. 2016;126(10):3961-3980.
41. Yamane K, Tateishi K, Klose RJ, et al. PLU-1 is an H3K4 demethylase involved in transcriptional repression and breast cancer cell proliferation. *Mol Cell*. 2007;25(6):801-812.
42. Tang B, Qi G, Tang F, et al. JARID1B promotes metastasis and epithelial-mesenchymal transition via PTEN/AKT signaling in hepatocellular carcinoma cells. *Oncotarget*. 2015;6(14):12723-12739.
43. Zhang T, Cooper S, Brockdorff N. The interplay of histone modifications - writers that read. *EMBO Rep*. 2015;16(11):1467-1481.
44. Quintas-Cardama A, Santos FP, Garcia-Manero G. Therapy with azanucleosides for myelodysplastic syndromes. *Nat Rev Clin Oncol*. 2010;7(8):433-444.
45. Jabbour E, Short NJ, Montalban-Bravo G, et al. Randomized phase 2 study of low-dose decitabine vs low-dose azacitidine in lower-risk MDS and MDS/MPN. *Blood*. 2017;130(13):1514-1522.

46. Kalac M, Scotto L, Marchi E, et al. HDAC inhibitors and decitabine are highly synergistic and associated with unique gene-expression and epigenetic profiles in models of DLBCL. *Blood*. 2011;118(20):5506-5516.
47. Laribi K, Denizon N, Ghnaya H, et al. Blastic plasmacytoid dendritic cell neoplasm: the first report of two cases treated by 5-azacytidine. *Eur J Haematol*. 2014;93(1):81-85.
48. Khwaja R, Daly A, Wong M, Mahe E, Cerquozzi S, Owen C. Azacitidine in the treatment of blastic plasmacytoid dendritic cell neoplasm: a report of 3 cases. *Leuk Lymphoma*. 2016;57(11):2720-2722.

Figure legends

Figure 1. The genomic characterization of BPDCN. (A) Circos plot graphical representation of the functional analysis performed on 54 genes recurrently mutated and/or affected by nonsense and frameshift SNVs in BPDCN WES samples. The four biological processes most significantly enriched are reported in the counterclockwise order from the highest to the lowest p-value: the gamma-aminobutyric acid (GABA) secretion (in violet), the Rac signaling (in red), the hematopoietic stem cell homeostasis (in light blue) and the epigenetic process (in green). The genes are colored according to their belonging to one or more of the biological process represented. In grey the genes not involved. (B) Overview of *ASXL1* and *TET2* mutations identified. Structure of ASXL1 protein with C-terminal plant homeodomain catalytic region and structure of TET2 protein showing the catalytic core region: the cysteine-rich (Cys) and double-stranded beta-helix (DSBH) domains. Empty circles: somatic SNVs. Symbols: “+” is for frameshift SNV and “*” for nonsense SNV. (C) Heatmap representation of SNVs in BPDCN WES samples and its distribution among selected pathways commonly mutated in myeloid disorders. The SNVs, the affected genes and the related pathways are reported in rows, while, the BPDCN samples in columns.

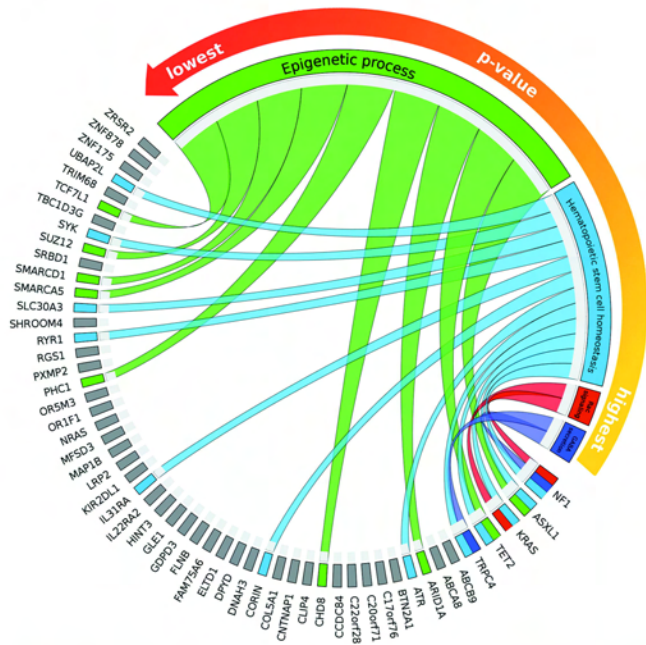
Figure 2

Figure 2. The transcriptome and H3K27 trimethylation/acetylation profiling of BPDCN. (A) Unsupervised hierarchical clustering performed on 5 BPDCN samples and 4 plasmacytoid dendritic cell (pDCs) samples according to the expression level of the RNA sequencing data. In the heat-map each row represents a gene and each column a sample. The color scale exemplifies the relative expression level of a gene across all samples: in red are represented genes with an expression level above the mean, in blue the genes with an expression level lower than the mean. Tumors (BPDCNs) and controls (pDCs) cluster in two distinct groups. (B) Gene Set Enrichment Analysis (GSEA) plot illustrates, in BPDCN patients the enrichment of the *KDM5B* and *PRMT5* gene signatures reported in literature³⁴⁻³⁶ as well as the enrichment of a set of genes, described by Missiaglia et al³⁷ as responsive to an hypomethylating treatment, namely Decitabine. *NES normalized enrichment score* ≥ 2 ; *FDR q-value false discovery rate* $\leq .0001$. (C) Visualization of anti-H3K27ac and anti-H3K27me3 normalized PAT-ChIP sequencing profiles in the UCSC Genome Browser showing genomic regions from patient BPDCN_25 and BPDCN_37. In the red boxes are indicated exemplificative regions displaying in both patients a similar level of anti-H3K27ac. Black solid rectangles represent genes in correspondence of the anti-H3K27ac peaks. (D) The Venn diagram shows that BPDCN_25 and BPDCN_37 patients shares 4542 H3K27ac promoters. (E) Histogram representation of the top 10 significant biological process emerged by Gene Ontology (GO) analysis of 86 upregulated genes marked by H3K27ac in their promoters. The GO categories are shown in x-axis and the fold enrichment values of observed versus expected genes are reported in the y-axis (*FDR qvalue* $< .001$).

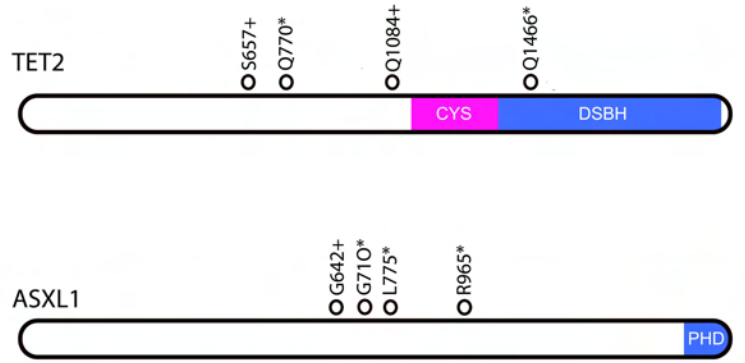
Figure 3

Figure 3. The efficacy of epigenetic agents in a preclinical BPDCN mouse model. (A) Pharmacodynamic assessment of the percentage of human CD56⁺CD38⁺ cells in the peripheral blood (PB), bone marrow (BM) of the femur and spine, spleen, and liver of a representative BPDCN mouse model vehicle-treated, after 39 days from CAL-1 injection. The cytofluorometric assays shows the tumor dissemination in all the tissues analysed. (B) Hematoxylin and eosin staining of bone marrow and spleen samples collected in a representative vehicle-treated NSG mouse at 39 days after CAL-1 injection (H&E; x400; Olympus DP2-SAL) . The histological assay shows a marked dissemination of blast elements. The immunohistochemistry detection of the CD303 (BDCA-2) antigen, in the murine bone marrow, indicates the presence of specific BPDCN blasts cells (Immuno-alkaline phosphatase; Gill's haematoxylin nuclear counterstaining; x400; Olympus DP2-SAL). (C) Graphical representation of the treatment schedules observed in BPDCN mouse model. Each treatment is represented by a single color or by a combination of colors and was administered for 4 weeks as follows: 5'-Azacytidine 5 mg/kg 5 doses at 2-day intervals (pink), Decitabine 2.5 mg/kg 3 doses at 2-day intervals (orange), Romidepsin 0.5 mg/kg every day (light blue), Bortezomib 0.5 mg/kg two times weekly (yellow). The same doses were administered in various combinations too. (D) Kaplan–Meier curves comparing overall survival of BPDCN mice models respectively treated with vehicle or the above reported treatments. Each treatment is summarized by a box colored as described above. The symbol “*” indicates that the combination of Decitabine and 5'-Azacytidine was the most effective in prolonging mice survival. Curves were compared by log-rank test, n= 5 mice/treatment arm. (E) Pharmacodynamic assessment of spleen size in four representative NSG mice CAL-1 injected after 39 days of treatment with vehicle (mouse Control), Decitabine (mouse Deci), 5'-Azacytidine (mouse Aza), and 5'-Azacytidine plus Decitabine (mouse Deci+Aza) according to the dosing schedule reported above.

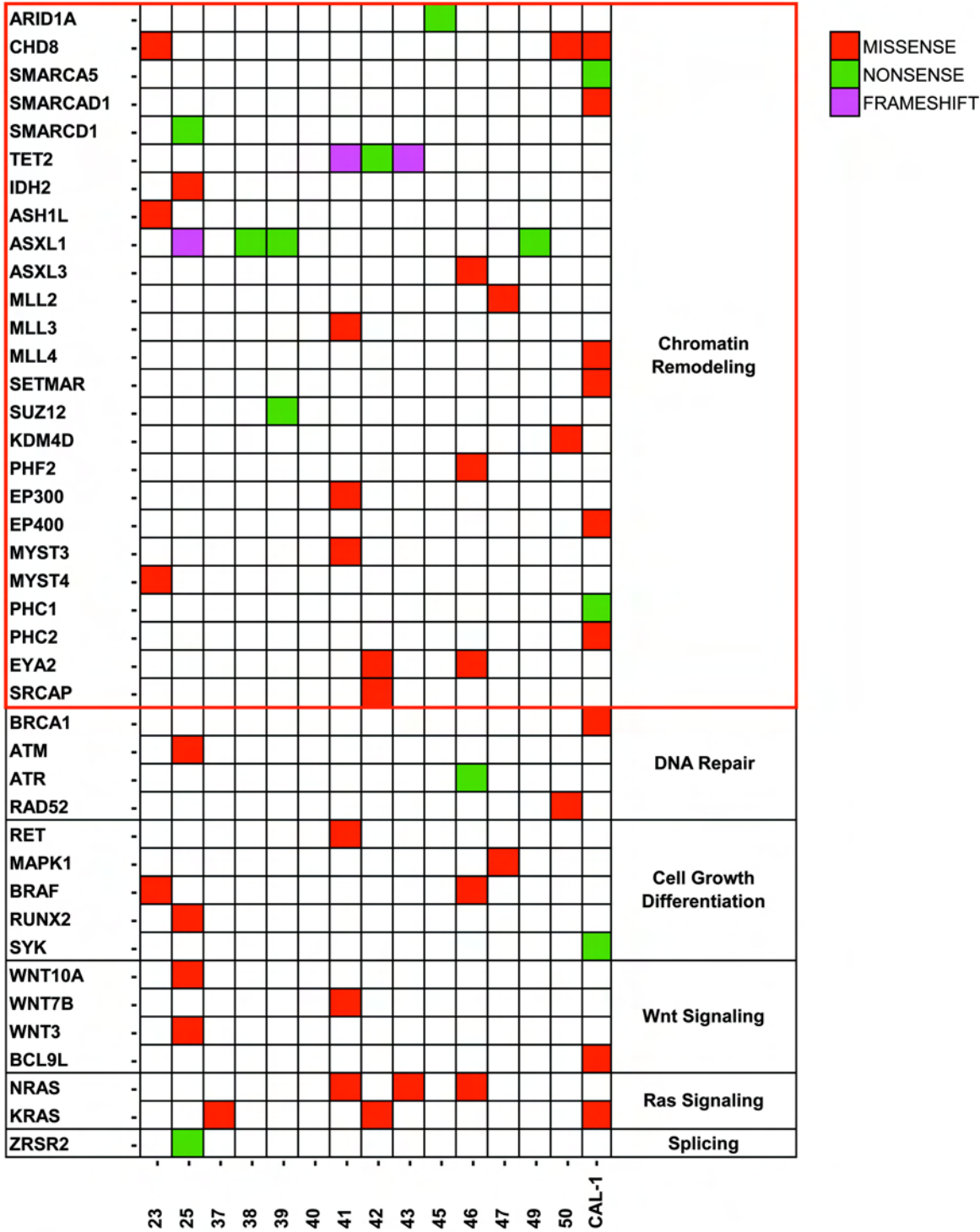
A

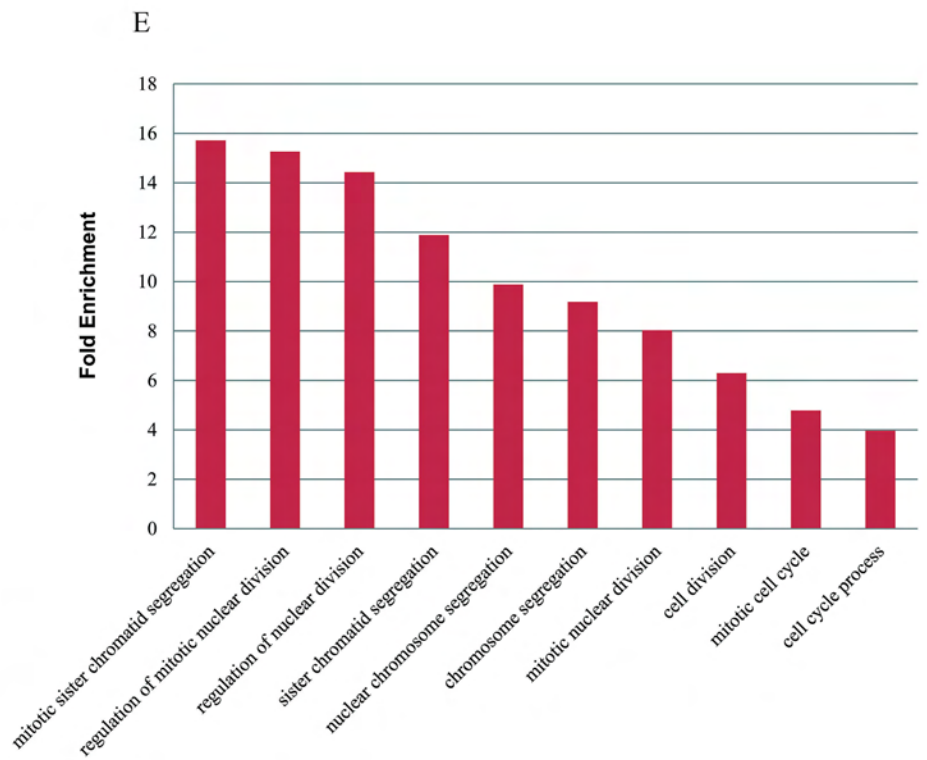
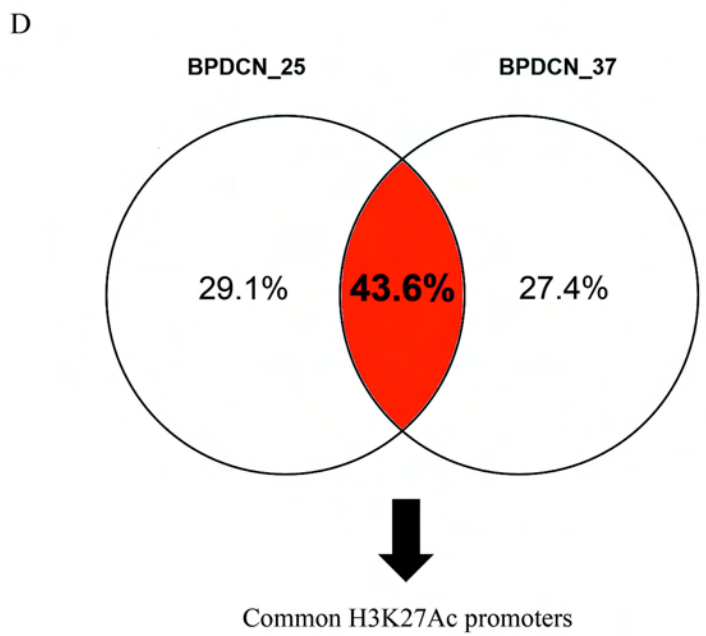
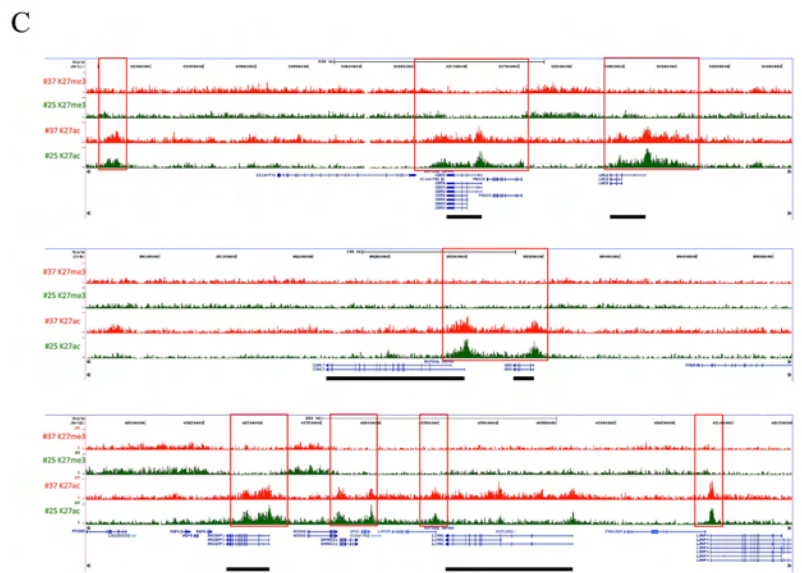
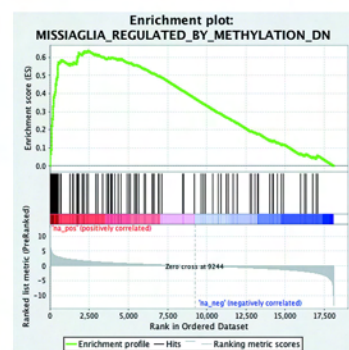
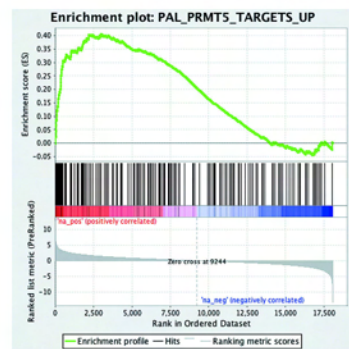
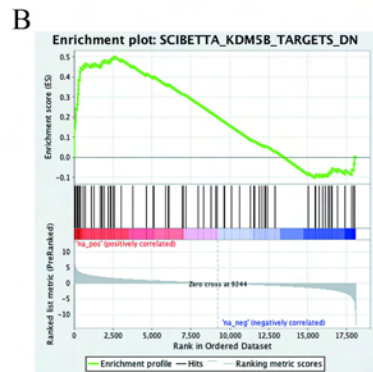
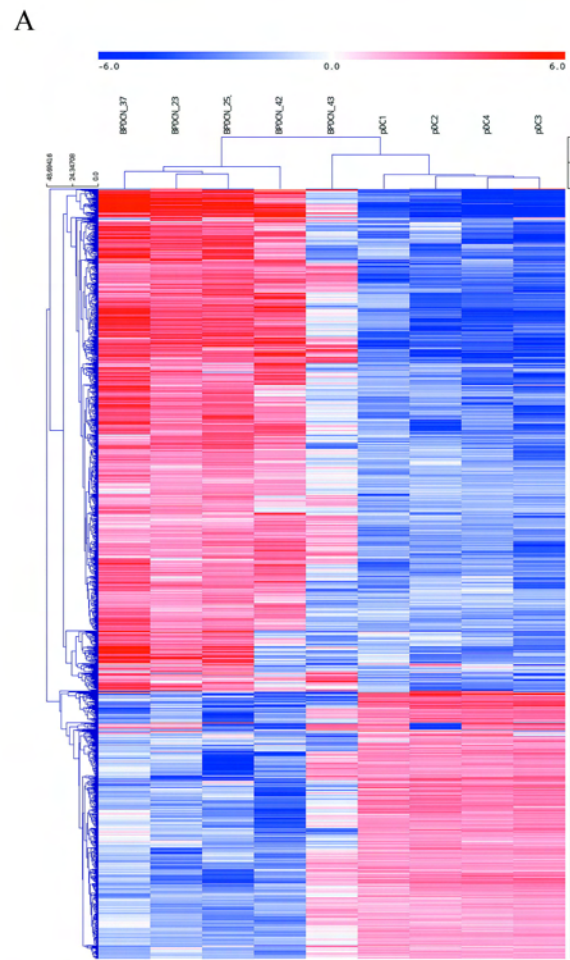


B

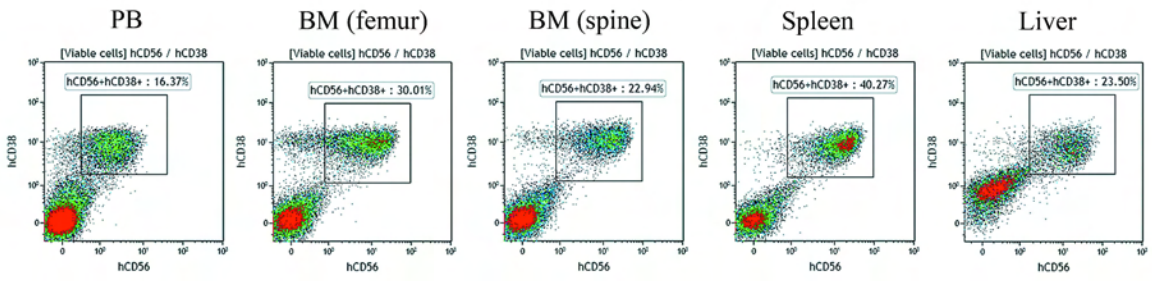


C

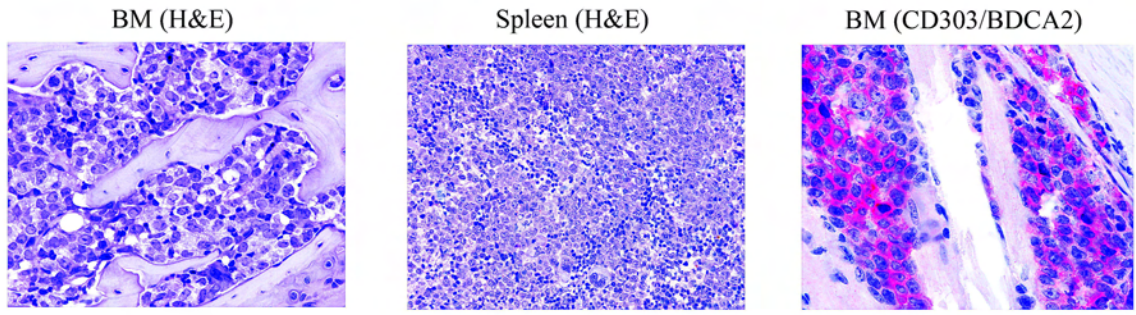




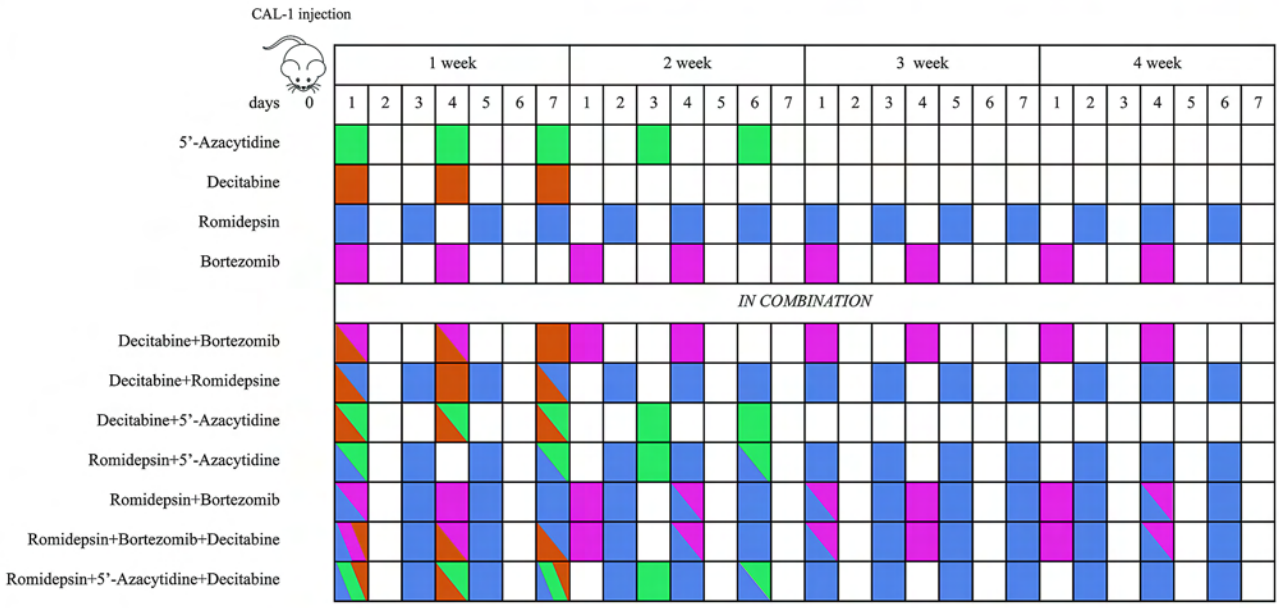
A



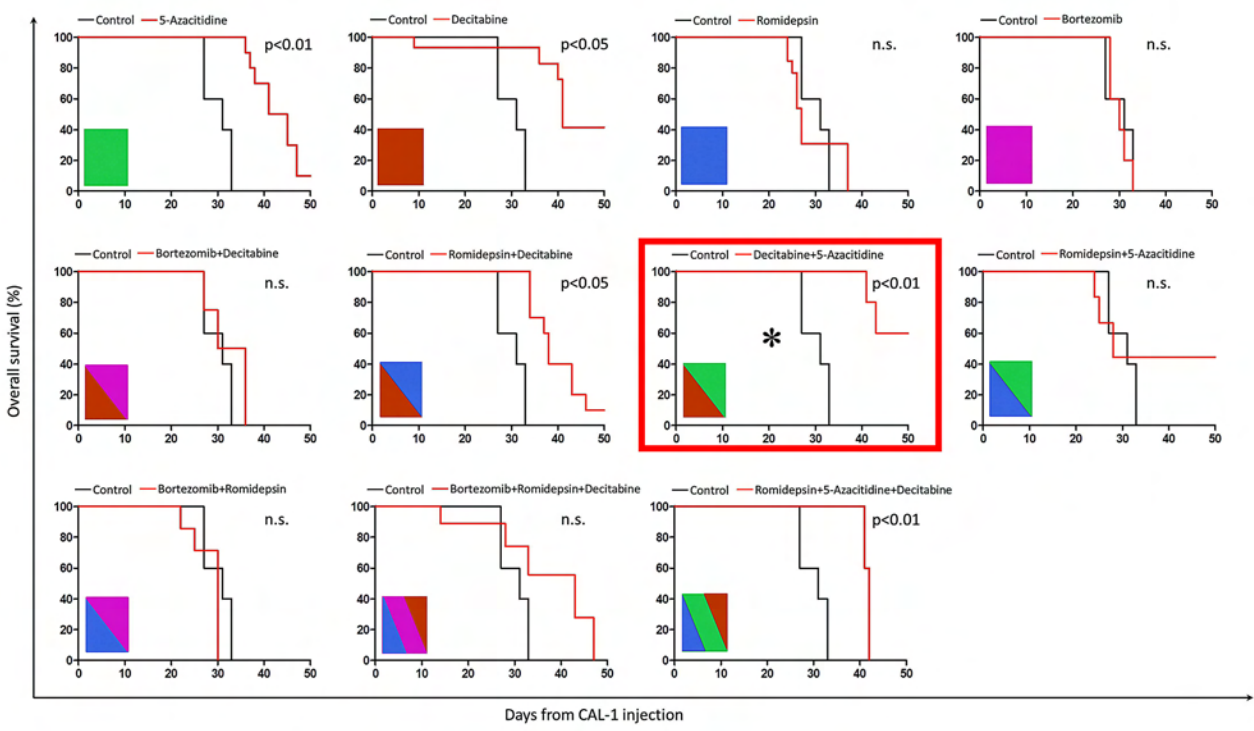
B



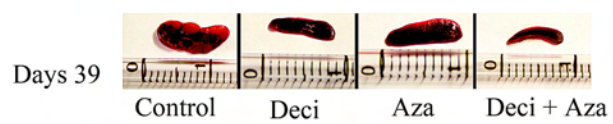
C



D



E



Supplementary Appendix

Immunohistochemistry and cytogenetics

Fourteen BPDCN cases were investigated and their clinical characteristics are reported in Table S1. All the skin biopsies at diagnosis were reviewed by a panel of at least three expert hematopathologists (CA, EB, FF, LC, MP, ES, CT, MT, and SAP) according to the WHO Classification criteria.¹ Immunohistochemistry (Dako Denmark) used the following antibodies: CD4,CD56, TdT (Novacastra) CD123 (BD Biosciences PharMingen), CD303/BDCA2 (Dendritics), TCL1 (Cell Marque), CD68PGM1, MPO, CD34, CD3, CD30 (Dako Denmark). If necessary, additional antibodies were evaluated accordingly to the specific requests of the single case (not reported). For the cytogenetic investigation of the BPDCN patients we used the whole exome sequencing data in order to map at highest resolution the chromosome 9 at cytoband p21 and evaluate the presence of the CDKN2A gene deletion in homo/heterozygosity; the most relevant alteration recognized by the WHO in the BPDCN context.

Immunohistochemistry and cytogenetic characteristics are summarized in Table S2.

DNA sample extraction

We used MagCore Genomic DNA Tissue Kit (RBC Bioscience Corp, Taiwan) for DNA extraction from cryopreserved tumoral skin biopsies, Oragene DNA kit (DNA Genotek Inc., ON, Canada) for DNA from saliva samples and MagCore Cultured Cells DNAKit (RBC Bioscience Corp, Taiwan) for DNA extraction from the CAL-1 cell line. All the samples were then loaded on the semi-automatic MagCore nucleic acid extractor (RBC Bioscience Corp, Taiwan). DNA quantity was evaluated by the Quant-iT PicoGreen dsDNA Assay Kit (Invitrogen Life technologies, UK) and all the samples passed the quality check.

Informed consent was obtained from each patient in accordance with the guidelines of the Institutional Review Board of the Department of Experimental, Diagnostic, and Specialty Medicine of the University of Bologna and the Declaration of Helsinki.

Whole Exome Sequencing (WES) libraries

Whole exome sequencing libraries were prepared by using the TruSeq Exome Kit (Illumina, San Diego, CA, USA) and Nextera Rapid Capture Exome kit (Illumina, San Diego, CA, USA). According to the kit instructions the genomic DNA of each patient was fragmented to provide DNA fragments with a base pair peak at 350 bp, ligated at the both ends with specific adapters and then purified by Agencourt AMPure XP beads (Beckman Coulter, Brea, CA, USA). The DNA was then amplified by ligation-mediated PCR, purified, and hybridized. Hybridized fragments bounded to streptavidin beads whereas non-hybridized fragments were washed out. Captured DNA library amplification products were assessed for quality by Agilent 7500 DNA assay (Agilent, Santa Clara, CA, USA) and quantified by Quant-iT PicoGreen dsDNA Assay Kit (Invitrogen Life technologies, UK), according to the manufacturer's protocol. Each captured library was subjected to cluster generation on cBot instrument (Illumina, Inc., San Diego, CA, USA) and finally paired-end sequencing was performed on the Illumina HiScan SQ platform (Illumina, San Diego, CA, USA) to generate 100 bp paired-end reads ($2 \times 100\text{PE}$). All the libraries passed the quality check.

Whole exome sequencing analysis

We performed paired-end sequencing of matched tumor/normal DNA samples (9 cases), tumor only DNA samples (5 cases), and the CAL-1 cell line (Table S3). Illumina HiScanSQ analysis produced an average of 70 million paired-end reads per sample. Average coverage breadth, defined as

the percentage of the captured coding sequence of a haploid reference covered by reads, was 98% (92% at 20x, 72% at 50x). We computed breadth of coverage using cnvkit (version 0.9.0), pysam (version 0.12.0.1) and samtools (version 1.6). Paired-end reads were mapped to the hg19 reference genome using the Burrows-Wheeler Aligner (BWA version 0.5.9)² alignment tool. We detected variants as sites that differed from the reference in each sample independently. To assess statistical significance of variant calling we used the SAVI algorithm (Statistical Algorithm for Variant Identification) developed at Columbia University.³ Briefly, SAVI constructs empirical priors for the distribution of variant frequencies for each sample. High-credibility intervals (posterior probability $\geq 1-10^{-5}$) are constructed for the corresponding change in frequency between tumor and normal samples. A discrete set of frequencies will be the base for constructing prior and posterior distribution and posterior probability is connected to the prior by a modified binomial likelihood. Variant with total depth in tumor and normal lower than 10x were filtered. Then, we first selected somatic variant with frequency greater than 10% in tumor samples and less than 3% in normal samples. In samples without a matched normal control we selected variants with depth greater than 20x and frequency greater than 25%. To remove systematic errors, we created an internal database with all the variants present in normal samples, and excluded all variants that were found to be present in any of the normal samples.

Functional Enrichment Analysis

To perform the functional mutation enrichment analysis, we selected only genes affected by deleterious SNVs (nonsense or frameshift) and/ or recurrently mutated in ≥ 3 samples, for a total of 54 genes. We analyzed the selected gene list by WebGestalt toolkit⁴, using the Overrepresentation Enrichment Analysis (ORA) method and the Gene Ontology/Biological Process functional database. In Table S7 the top 10 most significant biological processes emerged from the analysis.

Copy Number Analysis

We obtained copy number variation calls using cnvkit (version 0.9.0)⁵. Where possible, default parameters were used. We used GRCh37.75 human genome as reference. Starting from this reference, we built 10 kbases anti-target regions (as required by cnvkit). Then, we computed copy ratio, splitting the normal samples with respect to their exome sequencing preparation kit. The two normal reference copy number profiles were then used to estimate the copy ratio for the tumor samples. Finally, the copy ratios for each sample were discretized into absolute copy number calls using the “call” command of the cnvkit suite. Tumor purity (100% for the cell line, and 90% for the other samples) was the single parameter of the “call” step. For each sample and computation, we used the appropriate bedfile provided by each exome sequencing preparation kit: Nextera rapid capture exome kit (v1.2) and TruSeq Exome Kit (2012).

Sanger Sequencing

We validated by conventional Sanger sequencing two candidate nonsense somatic mutations of *SUZ12* and *ASXL1* occurring in the patients BPDCN_38 and BPDCN_39, respectively, as reported by WES analysis. We sequenced both tumor and normal DNA. The following PCR primers were custom-designed using Primer3 on line software (<http://bioinfo.ut.ee/primer3-0.4.0/primer3/>):

ASXL1-Forward-GGACTCACAGATGGGCTAGG, ASXL1-Reverse-AGAATGGGACCATTGTCTGC; SUZ12-Forward TCATGCCTGTATGCTGTTTG, SUZ12-Reverse- GAAGCAGATTCCCCCTTTTC.

The PCR products were sequenced both forward and reverse with ABI PRISM BigDye Terminator Cycle Sequencing Ready Reaction kit (Version 3) and loaded on ABI PRISM 3100-Avant Genetic Analyzer (Applied Biosystems, Foster City, CA, USA), according to manufacturer's instructions.

Tumor sequences were compared with the corresponding germline sequences using FinchTV version 1.4 software (Geospiza Inc., Seattle City, WA, USA).

Targeted sequencing libraries

We performed targeted sequencing of the 14 BPDCN tumor samples, 7 normal matched saliva samples, and the CAL-1 cell line (Supplemental Material, Table S4).

To validate the WES results we used the MiSeq TruSeq Custom Amplicon (Illumina, Inc., San Diego, CA, USA) a highly multiplexed targeted sequencing assay planned with DesignStudio, an online software, available at Illumina website. We developed a custom amplicon panel to specifically interrogate as many as 21 SNVs in 9 genes (Table S5). We used the TruSeq Custom Amplicon Kit with 250 ng of DNA per sample and the amplicon libraries were loaded on MiSeq instrument (Illumina, Inc., San Diego, CA, USA) to generate 2×151 -bp paired reads, according to the manufacturer's instructions. All libraries passed the quality check and the MiSeq targeted sequencing approach allowed us to reach a median coverage depth of 647X, a mean coverage depth of 1600X (ranging from 98X to 4056X).

Targeted sequencing analysis

Reads were aligned to the UCSC hg19 reference genome using BWA-MEM. Aligned reads were analyzed using the SAVI algorithm, and variants were selected based on coverage depth and frequency. Specifically, SAVI constructed empirical priors for the distribution of variant frequencies in each sample, from which we obtained a corresponding high-credibility interval for the frequency of a particular allele. To obtain estimates for

alleles with frequencies as low as 0.5%, we chose logarithmically spaced precision for the priors and posteriors. Furthermore, we considered variants detected in the normal samples and absent in the tumor as false positive calls and determined that alleles with lower bound interval of posterior probability less than 0.5 produced a false discovery rate $< 3\%$.

RNA sequencing libraries

Total RNA from the nine biopsies was extracted using TRIzol reagent (Invitrogen). Paired-end libraries (2x75 base pair) were prepared according to the TruSeq RNA sample preparation v2 protocol (Illumina, San Diego, USA). Briefly, 2 μg of Poly(A)⁺ RNA were purified from total RNA using poly-T oligo attached magnetic beads and then used for fragmentation into 130–290 bp fragments. First strand of cDNA synthesis was performed using reverse transcriptase enzyme (SuperScript II, Invitrogen, Life Technologies, USA) and random hexamer primer, followed by generation of double-stranded cDNA. AmpureXP beads (Beckman Coulter, Brea CA) were used to purify the ds cDNA and an End Repair step was performed to convert the overhangs, resulting from fragmentation, into blunt ends by 3' to 5' exonuclease activity. A single “A” nucleotide was added to the 3' ends of the blunt fragments to prevent them from ligating to one another during the adapter ligation reaction. This approach was adopted to ensure a low rate of chimera (concatenated template) formation. Subsequently, sequencing adapters were added to the ends of the ds cDNA fragment and a PCR reaction was used to selectively enrich those ds cDNA fragments that had adapter molecules on both ends, amplifying the amount of ds cDNA in the final libraries. Lastly, PCR library products were purified by AmpureXP beads and quality control analysis was assessed using a DNA-1000 (Agilent, USA). The quantification was performed by the Quant-it PicoGreen dsDNA Assay Kit per manufacturer's protocol (Invitrogen, Life

Technologies, USA). The resulting libraries were sequenced on an Illumina HiScan SQ (Illumina, San Diego, USA) following the manufacturer's instructions.

RNA sequencing analysis

We mapped 9 BPDCN samples – 5 cases belonging to the discovery set and 4 cases belonging to the extended set- by means of STAR aligner (version 2.4.0)⁶ on human reference genome hg19 and obtained an average of 70 million paired-end mapped reads per sample. Differential expression analysis and mRNA quantification was performed by means of DeSeq (Table S10).⁷

Gene set enrichment analysis was separately performed on the discovery and extended set by means of GSEA software and Molecular Signature Database (MSigDB)⁸ on the previously ranked gene list based on regularized base-2 DeSeq logarithm transformation.

Integration of RNA and PAT-ChIP sequencing

We recognized 86 genes up-regulated and also marked by H3K27acetylation. The Gene ontology Analysis was conducted on the 86 genes by WebGestalt toolkit,⁴ using the Overrepresentation Enrichment Analysis (ORA) method and the Gene Ontology/Biological Process functional database. In Table S11 the top 10 most enriched biological processes emerged from the analysis

Pathology tissue-chromatin immunoprecipitation (PAT-ChIP) sequencing

PAT-ChIP experiments were performed as in Fanelli *et al*⁹ with the following modification: sonication for chromatin extraction was performed in 400 ml. Antibodies used were: anti-Histone H3acetylK27 (ab472) and anti-trimethyl-Histone H3K27 (07-449). Immunoprecipitated DNA was

purified with QIAGEN columns and, after library preparation, sequenced with a HiSeq2000 in multiplexed run to obtain 50 bp single-end reads following manufacturer protocols. FASTQ files were quality checked and filtered with NGS QC Toolkit (version 2.3.3) using default parameters. Alignments were performed with Burrows-Wheeler Aligner (version 0.7.10)² to hg18 using default parameters. SAMtools (version 1.2) and BEDtools (version 2.24) were used for filtering steps and file formats conversion. Duplicate reads were discarded and peaks were identified from uniquely mapping reads, using MACS (version 2.1.0) callpeak with default parameters and -broad, -SPMR, -shiftsize 73 options. The q-value cutoff used to call significant regions was 0.05. UCSC tools and genome browser was used for data visualization.

ChIP-seq signals of peaks called by MACS were subjected to unbiased clustering, using the seqMINER 1.3.2 platform.¹⁰ Linear Kmeans was used for clustering, with the following parameters: left and right extension = 5 kb, internal bins (with respect to the peaks) = 160, number of cluster = 25. seqMINER was also used to generate the heatmaps and the average profiles of read density for the different clusters.

Mouse Model

Experiments were carried out on nonobese diabetic severe combined immunodeficient NOD/SCID interleukin-2 receptor γ (IL-2R γ)-null (NSG) mice, 6 to 8 weeks old. NSG mice were bred and housed under pathogen-free conditions in the animal facilities at the European Institute of Oncology–Italian Foundation for Cancer Research (FIRC) Institute of Molecular Oncology (IEO-IFOM, Milan, Italy) as previously reported.¹¹ All animal experiments were carried out in accordance with the applicable Italian laws (D.L.vo 26/14 and following amendments) and the institutional guidelines. All *in vivo* studies were ratified by the Italian Ministry of Health. For induction of BPDCN in mice, 5.000 CAL-1 cells were injected intravenously (i.v.) through the lateral tail vein in non-irradiated mice. Human engraftment was defined by means of percentage of human cells in peripheral blood from tail vein of the recipient animals.

Human cell engraftment in the peripheral blood, bone marrow of the femur and of the spine, spleen and liver was investigated by flow cytometry and immunohistochemistry from 39 days after transplant onward in a representative mouse vehicle-treated. The phenotype of human cells in NSG mice was evaluated by flow cytometry using the following anti-human antibodies: anti-CD38-APC (clone LS198-4-3), -CD45-APC-Cy7 (clone J33), -CD56-PE (clone N901) from Beckman-Coulter and anti-mouse CD45-FITC (clone 30-F11) from Becton Dickinson (BD) to exclude murine cell contamination from the analysis. After red cell lysis, cell suspensions were evaluated by a FACSCalibur (BD) using analysis gates designed to exclude dead cells, platelets and debris. Percentages of stained cells were determined and compared to appropriate negative controls. Seven-aminoactinomycin D (7AAD; Sigma-Aldrich) was used to enumerate viable, apoptotic and dead cells. Hematoxylin and eosin (H&E) staining was performed on the bone marrow and spleen of transplanted mice vehicle-treated after 39 days. Immunohistochemistry was performed on samples

obtained from the spine of transplanted mice vehicle-treated after 39 days by using an anti-BDCA2/CD303 antibody (Dendritics, Lyon, France; Clone 124B3; dilution: 1:20). The test was carried out as previously described.¹¹

In vivo treatments

Bortezomib, 5'-Azacytidine, Decitabine provided by Sigma-Aldrich (Sigma-Aldrich Corporation, St. Louis, MO, USA) and Romidepsin provided by Santa Cruz (Santa Cruz Biotechnology, Santa Cruz, CA), were dissolved in saline (0.9% w/v NaCl) and injected intraperitoneally into the mice: Bortezomib was administrated at 0.5 mg/kg two times weekly for 4 weeks, 5'-Azacytidine 5 mg/kg 5 doses (2-day intervals), Decitabine 2.5 mg/kg 3 doses (2-day intervals) and Romidepsin 0.5 mg/kg every day for 4 weeks. Drug dosages were previously defined as non-toxic in mice not injected with CAL-1. Administration started one day after CAL-1 cells injection. Mice were monitored for survival daily until reaching humane end-points. The log-rank test was used to compare survival between different groups. All experiments were carried out in duplicate, a total of 110 animals having been treated.

Table S1. Patients clinical characteristics

Sample	Sex	Age (Y)	Tissue	Other sites	F. Up	(mo)	Main Therapy	Transplant
BPDCN_40	F	9	Skin	BM	DOD	71.5	AIEOP AML 2002/HR	Auto-SCT
BPDCN_39	M	89	Skin	NA	LOST	NA	NA	NA
BPDCN_23	M	19	Skin	//	DOD	76	CHOP + MTX	Allo-SCT
BPDCN_43	M	67	Skin	BM, LN	DOD	6.3	GIFOX	NO
BPDCN_25	M	62	Skin	BM, PB, LN	ADF	21	Hyper-CVAD	NO
BPDCN_45	F	66	Skin	LN	DOD	36	Hyper-CVAD	Auto-SCT
BPDCN_46	M	29	Skin	PH	ADF	57	Hyper-CVAD	Auto-SCT
BPDCN_41	M	60	Skin	//	DOD	41.3	ICE	Auto + Allo-SCT
BPDCN_47	M	78	Skin	//	ADF	74	Local RT	NO
BPDCN_49	F	49	Skin	//	DOD	28	Local RT	NO
BPDCN_42	F	73	Skin	BM, PB, LN, PL	DOD	7.6	MICE	NO
BPDCN_37	M	75	Skin	NA	DOD	9	NA	NA
BPDCN_38	M	69	Skin	BM	DOD	6.4	NILG AML 02/06	Allo-SCT
BPDCN_50	M	37	Skin	LN	LOST	NA	NA	NA

Abbreviations: BPDCN, blastic plasmacytoid dendritic cell neoplasm; y, years; mo, months; M, male; F, female; BM, bone marrow; LN, lymph node, PB, peripheral blood; PH, pharynx; PL, pleura; DOD, died of disease; AWD, alive with disease; ADF, alive disease free; LOST, lost at follow-up; NA, not available. AIEOP AML 2002/HR, Associazione Italiana di Ematologia e Oncologia Pediatrica acute myeloid leukemia high-risk children 2002/01 trial; CHOP, cyclophosphamide, doxorubicin, vincristine, prednisone; CHOP+MTX, cyclical chemotherapy with high-dose methotrexate and CHOP; GIFOX, gemcitabine, ifosfamide, and oxaliplatin; Hyper-CVAD, alternate cycles of hyper-fractionated cyclophosphamide, vincristine, doxorubicin, dexamethasone, and methotrexate and cytarabine; ICE, idarubicin, cytarabine, etoposide; RT, radiotherapy; MICE, mitoxantrone, cytarabine, etoposide; NILG AML 02/06, Northern Italy Leukemia Group acute myeloid leukemia 02/06 trial; Auto-SCT, autologous stem cell transplant; Allo-SCT, allogenic stem cell transplant.

Table S2 . Patients immunohistochemical and cytogenetic characteristics

Case No	CD3	CD4	CD30	CD34	CD56	CD68PGM1	CD123	CD303/BDCA2	TCL1	MPO	TdT	DEL_CDKN2A Y/N
BPDCN_23	(-)	(+)	(-)	(-)	(+)	(+ -)	(+)	(+)	(+)	(-)	(-)	Y homozygosity
BPDCN_25	na	(+)	na	(-)	(+)	(+ -)	(+)	(+)	(+)	(-)	(-)	Y heterozygosity
BPDCN_37	(-)	(+)	na	na	(+)	(- +)	(+)	na	na	(-)	(-)	N
BPDCN_38	(-)	(+)	na	(-)	(+ -)	(- +)	(+)	(+)	(+)	(-)	na	Y heterozygosity
BPDCN_39	(-)	(+ -)	(-)	(-)	(+)	(- +)	(+)	(+)	na	na	(-)	Y heterozygosity
BPDCN_40	na	(- +)	na	(-)	(+)	na	(+)	(+)	(- +)	na	(+ -)	N
BPDCN_41	(-)	(+)	(-)	(- +)	(+ -)	(- +)	(+)	(+)	(+ -)	(-)	(-)	N
BPDCN_42	na	(+)	na	na	(+)	na	(-)	(+)	na	na	na	Y homozygosity
BPDCN_43	(- +)	(-)	(-)	(-)	(+)	na	(+)	(+)	na	(-)	(-)	N
BPDCN_45	(-)	(- +)	na	(-)	(+ -)	(- +)	(+ -)	(+)	(+)	(-)	(-)	N
BPDCN_46	(-)	(+)	(-)	(- +)	(+)	(- +)	(+)	na	(-)	na	na	Y heterozygosity
BPDCN_47	(-)	(+ -)	(-)	(-)	(+)	(+ -)	(+)	(+)	(+ -)	(-)	(-)	N
BPDCN_49	(-)	(+)	(-)	(-)	(+)	(-/ +)	(+)	na	na	(-)	(-)	Y heterozygosity
BPDCN_50	(-)	(+)	na	(-)	(+)	(-/ +)	(+)	(-)	na	(-)	(-)	Y homozygosity

Abbreviations: BPDCN, blastic plasmacytoid dendritic cell neoplasm; (+), positive > 75% cells ; (+ -), positive 50-75% cells; (- +), positive 25-50%; (-), negative, no cell; DEL, deletion.

Table S3. BPDCN samples sequenced by Whole-Exome Sequencing.

Sample	Wes	Tumor cells %
BPDCN_37	Matched	≥90%
BPDCN_38	Matched	≥90%
BPDCN_39	Matched	≥90%
BPDCN_40	Matched	≥90%
BPDCN_43	Matched	≥90%
BPDCN_45	Matched	≥90%
BPDCN_46	Matched	≥90%
BPDCN_47	Matched	≥90%
BPDCN_49	Matched	≥90%
BPDCN_23	Unmatched	≥90%
BPDCN_25	Unmatched	≥90%
BPDCN_41	Unmatched	≥90%
BPDCN_42	Unmatched	≥90%
BPDCN_50	Unmatched	≥90%
CAL-1	Unmatched	100%

Abbreviations: BPDCN, blastic plasmacytoid dendritic cell neoplasm; CAL-1, blastic plasmacytoid dendritic cell line

Table S4. BPDCN samples sequenced by MiSeq targeted sequencing.

Sample	MiSeq	Tumor cells %
BPDCN_37	matched	≥90%
BPDCN_39	matched	≥90%
BPDCN_40	matched	≥90%
BPDCN_43	matched	≥90%
BPDCN_45	matched	≥90%
BPDCN_46	matched	≥90%
BPDCN_49	matched	≥90%
BPDCN_23	unmatched	≥90%
BPDCN_25	unmatched	≥90%
BPDCN_38	unmatched	≥90%
BPDCN_41	unmatched	≥90%
BPDCN_42	unmatched	≥90%
BPDCN_47	unmatched	≥90%
BPDCN_50	unmatched	≥90%
CAL-1	unmatched	100%

Abbreviations: BPDCN, blastic plasmacytoid dendritic cell neoplasm; CAL-1, blastic plasmacytoid dendritic cell line

Table S5. The genes investigated by MiSeq targeted sequencing.

Genes	Regions selected for Miseq panel
<i>IDH2</i>	Hot spot region (Ex 4)
<i>KRAS</i>	Hot spot region (Ex 2, 3)
<i>BRAF</i>	Hot spot region (Ex 11, 15)
<i>ZRSR2</i>	All coding Exons
<i>TET2</i>	All coding Exons
<i>TNFRSF13B</i>	All coding Exons
<i>ASXL1</i>	All coding Exons
<i>SUZ12</i>	All coding Exons
<i>NRAS</i>	Only Exon 2

Table S6. MiSeq targeted sequencing validation results.

Cases	Frequency %	ref/var	Gene	CCDS	AA	Validation MiSeq Y/N
BPDCN_25	28	-/G	<i>ASXL1</i>	CCDS13201.1	G642+	Y
BPDCN_38	55	G/T	<i>ASXL1</i>	CCDS13201.1	G710*	Y
BPDCN_39	36	T/A	<i>ASXL1</i>	CCDS13201.1	L775*	Y
BPDCN_49	10	C/T	<i>ASXL1</i>	CCDS13201.1	R965*	Y
BPDCN_47	49	A/G	<i>ASXL1</i>	CCDS13201.1	N986S	Y
BPDCN_41	41	-/A	<i>TET2</i>	CCDS47120.1,CCDS3666.1	S657+	Y
BPDCN_42	27	C/T	<i>TET2</i>	CCDS47120.1,CCDS3666.1	Q770*	Y
BPDCN_38	33	G/A	<i>TET2</i>	CCDS47120.1,CCDS3666.1	W1003*	Y
BPDCN_43	51	-/A	<i>TET2</i>	CCDS47120.1,CCDS3666.1	Q1084+	Y
BPDCN_42	41	C/T	<i>TET2</i>	CCDS47120.1	Q1466*	Y
BPDCN_37	80	C/T	<i>TET2</i>	CCDS47120.1	R1516*	Y
BPDCN_42	33	C/G	<i>KRAS</i>	CCDS8702.1,CCDS8703.1	L19F	Y
BPDCN_CAL-1	99	C/G	<i>KRAS</i>	CCDS8702.1,CCDS8703.1	G12A	Y
BPDCN_43	34	C/G	<i>NRAS</i>	CCDS877.1	G12A	Y
BPDCN_41	32	C/T	<i>NRAS</i>	CCDS877.1	G12S	Y
BPDCN_23	38	C/G	<i>BRAF</i>	CCDS5863.1	G469A	Y
BPDCN_46	25	C/A	<i>BRAF</i>	CCDS5863.1	G464V	N
BPDCN_39	42	C/T	<i>SUZ12</i>	CCDS11270.1	R654*	Y
BPDCN_50	42	C/T	<i>TNFRSF13B</i>	CCDS11181.1	R122Q	Y
BPDCN_25	90	C/G	<i>ZRSR2</i>	CCDS14172.1	Y373*	Y
BPDCN_25	40	C/T	<i>IDH2</i>	CCDS10359.1	R140Q	Y

Table S7. Top 10 biological processes emerged from gene functional analysis of WES data

Term	Description	Count	P-value	FDR	Fold Enrich.
EPIGENETIC PROCESS					
GO:0016569	covalent chromatin modification	8	0.000101184	0.333669805	5.362358277
GO:0006325	chromatin organization	9	0.000117091	0.333669805	4.586177715
GO:0048096	chromatin-mediated maintenance of transcription	2	0.000332385	0.473593505	72.25777778
GO:0045815	positive regulation of gene expression, epigenetic	3	0.000470088	0.519119857	19.70666667
HEMATOPOIETIC STEM CELL HOMEOSTASIS					
GO:0061484	hematopoietic stem cell homeostasis	2	0.000111579	0.333669805	120.4296296
GO:0042592	homeostatic process	13	0.000284612	0.473593505	2.928151843
RAC SIGNALING					
GO:0035020	regulation of Rac protein signal transduction	2	0.000485783	0.519119857	60.21481481
GABA SECRETION					
GO:0014051	gamma-aminobutyric acid secretion	2	0.000266377	0.473593505	80.28641975
GO:0015812	gamma-aminobutyric acid transport	2	0.000573097	0.54437804	55.58290598

Table S8. SNVs of *ASXL1* and *TET2* genes.

Gene	SNV	DNA	Sample	AA	SNV	Position	COSMIC
<i>TET2</i>	Somatic	Unmatched	BPDCN_41	S657+	frameshift	before interaction with DNA domain	//
	Somatic	Unmatched	BPDCN_42	Q770*	nonsense	before interaction with DNA domain	//
	Somatic	Matched	BPDCN_43	Q1084+	frameshift	before interaction with DNA domain	//
	Somatic	Unmatched	BPDCN_42	Q1466*	nonsense	before interaction with DNA domain	//
<i>ASXL1</i>	Somatic	Unmatched	BPDCN_25	G642+	frameshift	inside interaction with NCOA1 domain	COSM G642*
	Somatic	Matched	BPDCN_38	G710*	nonsense	before domain for interaction with RARA	COSM1283534
	Somatic	Matched	BPDCN_39	L775*	nonsense	before domain for interaction with RARA	COSM52930
	Somatic	Matched	BPDCN_49	R965*	nonsense	before domain for interaction with RARA	COSM132978

Table S9. Twenty-five epigenetic modifier genes mutated in BPDCN.

Case	chr:pos	ref/var	Gene	AA	Cosmic_v66_ Gene	MutComFocal Mut Score	Polyphen2 HDIV_score	Polyphen2 HVAR_score	SIFT_score
BPDCN_45	chr1:27106539	G/A	<i>ARID1A</i>	W1833*	790	1.66E-05 1
BPDCN_23	chr1:155448058	G/A	<i>ASHIL</i>	R1535C	273	5.00E-07	1.0;1.0	0.99;0.996	0
BPDCN_25	chr20:31022441	-/G	<i>ASXL1</i>	G642+	849	5.43E-04	.	.	0.15
BPDCN_38	chr20:31022643	G/T	<i>ASXL1</i>	G710*	849	5.43E-04	.	.	1
BPDCN_39	chr20:31022839	T/A	<i>ASXL1</i>	L775*	849	5.43E-04	.	.	0.67
BPDCN_49	chr20:31023408	C/T	<i>ASXL1</i>	R965*	849	5.43E-04	0.009;0.009	0.005;0.005	0.45
BPDCN_47	chr20:31023472	A/G	<i>ASXL1</i>	N986S	849	5.43E-04	0.208	0.029	0.13
BPDCN_46	chr18:31323569	C/T	<i>ASXL3</i>	P1253S	131	1.15E-06	0.999	0.988	0
BPDCN_50	chr14:21854308	G/A	<i>CHD8</i>	R2125W	205	5.87E-06	0.004	0.003	0.71
BPDCN_23	chr14:21861393	G/A	<i>CHD8</i>	L1835F	205	5.87E-06	0.999;0.999 .	0.997;0.995 .	0.02 .
BPDCN_CAL-1	chr14:21873903	C/T	<i>CHD8</i>	G731R	205	5.87E-06	.	.	1
BPDCN_CAL-1	chr4:144457820	T/G	<i>SMARCA5</i>	L495*	72	3.68E-07	0.028;0.021	0.004;0.009	0.43
BPDCN_CAL-1	chr4:95173830	A/C	<i>SMARCAD1</i>	N318T	92	5.64E-07	.	.	0.2
BPDCN_25	chr12:50492757	C/T	<i>SMARCD1</i>	Q508*	35	1.60E-06	.	.	1
BPDCN_39	chr17:30325762	C/T	<i>SUZ12</i>	R654*	54	5.58E-05	0.286;0.165;0.009	0.055;0.02;0.003	0.21
BPDCN_CAL-1	chr3:4345101	A/G	<i>SETMAR</i>	E16G	30	1.34E-06	0.988;0.979	0.794;0.628	0.09
BPDCN_42	chr16:30732644	C/T	<i>SRCAP</i>	P1130S	275	6.08E-07	2.90E-04	.	0.34
BPDCN_41	chr4:106157069	-/A	<i>TET2</i>	S657+	929	2.90E-04	.	.	1
BPDCN_42	chr4:106157407	C/T	<i>TET2</i>	Q770*	929	2.90E-04	.	.	0.25
BPDCN_38	chr4:106158108	G/A	<i>TET2</i>	W1003*	929	2.90E-04	.	.	1
BPDCN_43	chr4:106158349	-/A	<i>TET2</i>	Q1084+	929	2.90E-04	.	.	1
BPDCN_42	chr4:106193934	C/T	<i>TET2</i>	Q1466*	929	2.90E-04	.	.	0.25
BPDCN_37	chr4:106196213	C/T	<i>TET2</i>	R1516*	929	2.90E-04	1	0.998	0
BPDCN_25	chr15:90631934	C/T	<i>IDH2</i>	R140Q	607	3.04E-06	1	1	0
BPDCN_47	chr12:49448165	C/G	<i>MLL2</i>	W145C	600	1.51E-05	1	1	0
BPDCN_41	chr7:151843784	A/C	<i>MLL3</i>	V4644G	774	1.51E-06	. 0.993;0.804;0.902	. 0.907;0.342;0.415	0.02 0.01

BPDCN_CAL-1	chr19:36216708	C/T	<i>MLL4</i>	R1292W	223	1.07E-06	1	0.981	0
BPDCN_50	chr11:94731791	C/T	<i>KDM4D</i>	R419W	54	2.46E-06	0.002	0.001	0.01
BPDCN_46	chr9:96429387	C/T	<i>PHF2</i>	S738L	105	1.64E-06	0.064;0.002	0.005;0.001	0.21
BPDCN_CAL-1	chr12:9085218	C/T	<i>PHC1</i>	Q389*	65	5.63E-07	.	.	0.15
BPDCN_CAL-1	chr1:33836638	C/A	<i>PHC2</i>	A131S	72	7.53E-07	0.009;0.009;0.049	0.014;0.006;0.012	1
BPDCN_41	chr22:41573648	G/C	<i>EP300</i>	G1978A	326	9.51E-07	0.734	0.196	0.46
BPDCN_CAL-1	chr12:132445627	C/T	<i>EP400</i>	P155S	346	4.73E-07	0.196;0.121;0.196;0.245;0.036	0.044;0.044;0.044;0.094;0.028	0.16
BPDCN_CAL-1	chr12:132471135	C/A	<i>EP400</i>	S668Y	346	4.73E-07	0.631;0.631;0.631;0.98;0.753	0.329;0.329;0.329;0.851;0.329	0.05
BPDCN_46	chr20:45618703	T/A	<i>EYA2</i>	D18E	71	1.12E-05	0.0;0.0;0.0;0.0	0.001;0.001;0.001;0.001	0.8
BPDCN_42	chr20:45702876	C/T	<i>EYA2</i>	P188L	71	1.12E-05	0.996;0.846;0.875;0.875	0.797;0.131;0.173;0.173	0.02
BPDCN_41	chr8:41789947	T/C	<i>MYST3</i>	M1931V	193	4.16E-06	0.969	0.914	0.15
BPDCN_23	chr10:76784746	C/T	<i>MYST4</i>	R1135C	209	2.84E-06	1.0;1.0;1.0	0.997;0.998;0.988	0

Table S10. Samples analyzed by RNA sequencing.

Sample	WES	Set	Tumor cells %
BPDCN_21	N	Extension Set	≥90%
BPDCN_20	N	Extension Set	≥90%
BPDCN_22	N	Extension Set	≥90%
BPDCN_24	N	Extension Set	≥90%
BPDCN_23	Y	Discovery Set	≥90%
BPDCN_25	Y	Discovery Set	≥90%
BPDCN_37	Y	Discovery Set	≥90%
BPDCN_42	Y	Discovery Set	≥90%
BPDCN_43	Y	Discovery Set	≥90%
pDC_1	N	Both	//
pDC_2	N	Both	//
pDC_3	N	Both	//
pDC_4	N	Both	//

Abbreviations: BPDCN, blastic plasmacytoid dendritic cell neoplasm; pDC, plasmacytoid dendritic cells; samples already sequenced by WES Y, yes; N, no.

Table S11. Top 10 significant biological process emerged by Gene Ontology analysis of 86 up-regulated genes marked by H3K27-promoter acetylation

Term	Description	Count	P-Value	Fold Enrichment	FDR
GO:0007067	mitotic nuclear division	15	3.69034691694026e-10	8.027320606	3.15487757929223e-06
GO:0007059	chromosome segregation	13	1.26807986333688e-09	9.177333912	3.71276365696005e-06
GO:0051783	regulation of nuclear division	10	1.63092095384343e-09	14.42590949	3.71276365696005e-06
GO:0000819	sister chromatid segregation	11	1.8299290971413e-09	11.88292359	3.71276365696005e-06
GO:0098813	nuclear chromosome segregation	12	2.55158560946711e-09	9.883282675	3.71276365696005e-06
GO:0000278	mitotic cell cycle	20	2.60575294674936e-09	4.778953557	3.71276365696005e-06
GO:0000070	mitotic sister chromatid segregation	9	5.32755506377214e-09	15.71664876	6.50646689145543e-06
GO:0007088	regulation of mitotic nuclear division	9	6.9189063367503e-09	15.25776851	7.39371628410979e-06
GO:0051301	cell division	15	1.00188266571877e-08	6.299922501	9.0508192280403e-06
GO:0022402	cell cycle process	22	1.05869917277346e-08	3.967125111	9.0508192280403e-06

Supplemental Figures

Figure S1. Sanger Sequencing validation experiments. Representative chromatograms of matched tumor DNA samples and germline DNA of saliva samples showing somatic mutations in exon 13 and exon 16 of *ASXL1* and *SUZ12* of two patients, respectively. Mutations were detected in both strands of tumor DNA and absent from germline DNA.

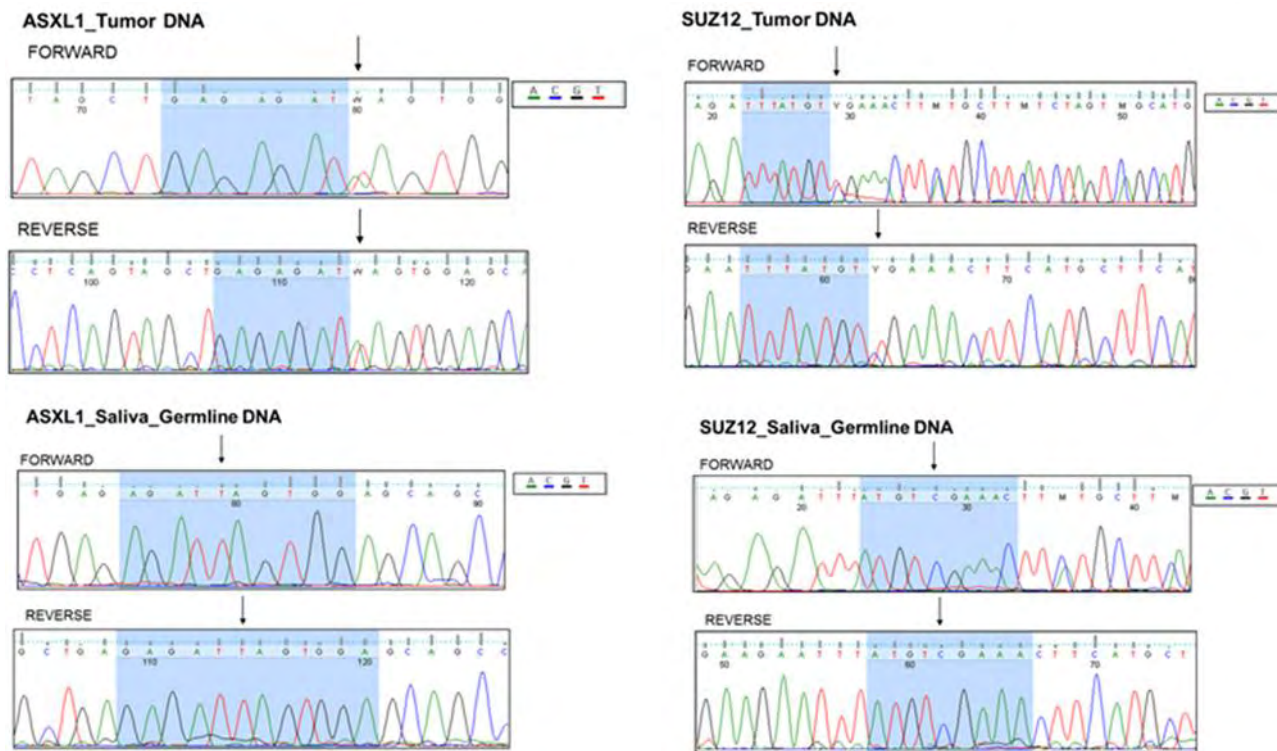


Fig.S2 - Chromosome 9 copy ratio heatmap. Blu color represents chromosome segment loss (homozygous deletion is darker than single-copy loss). Red color represents chromosome segment gain. Values of this heatmap are the ratios between each tumor sample segment with respect to the corresponding normal reference segment. . (BPDCN_01_U represent the CAL-1 tumor cell line) . Therefore, a lower ratio (negative number) means that the tumor sample segment is less represented with respect to the corresponding normal reference segment.

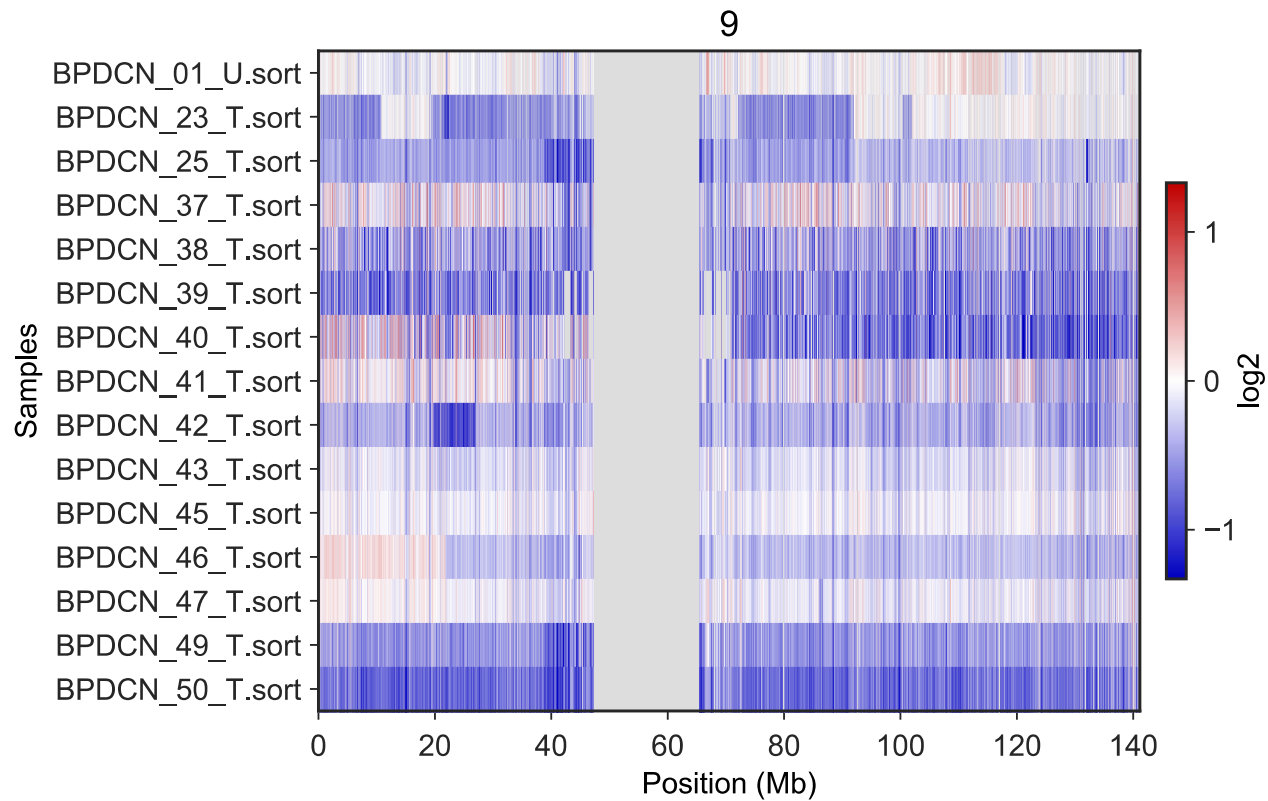


Figure S3. Copy number variants of 9 recurrently mutated genes (≥ 3 BPDCN samples). Each row represents a gene and each column a BPDCN sample.

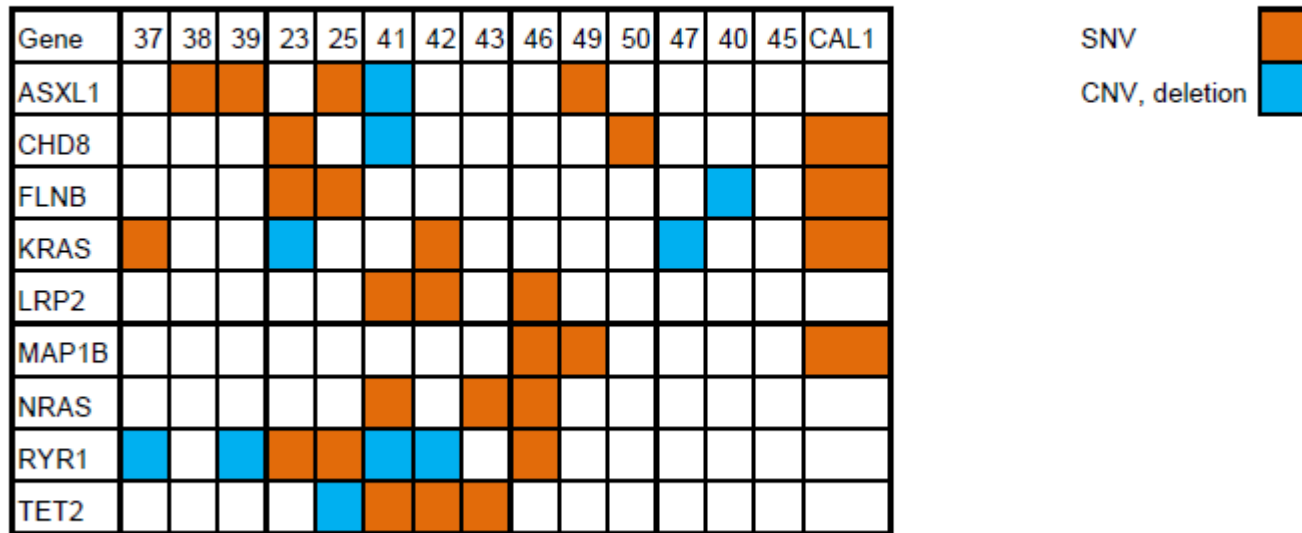


Figure S4 Gene Set Enrichment Analysis (GSEA) in BPDCNs extension set . Representative plots illustrate, in BPDCN patients the enrichment of the same gene signatures recognized also in BPDCN discovery set: the *KDM5B* and *PRMT5* gene signatures reported in literature^{12,13} and also the enrichment of a set of genes, described by Missiaglia *et al*¹⁴ as responsive to a hypomethylating treatment, namely the Decitabine. NES normalized enrichment score ≥ 1.8 ; FDR q-val. false discovery rate ≤ 0.02

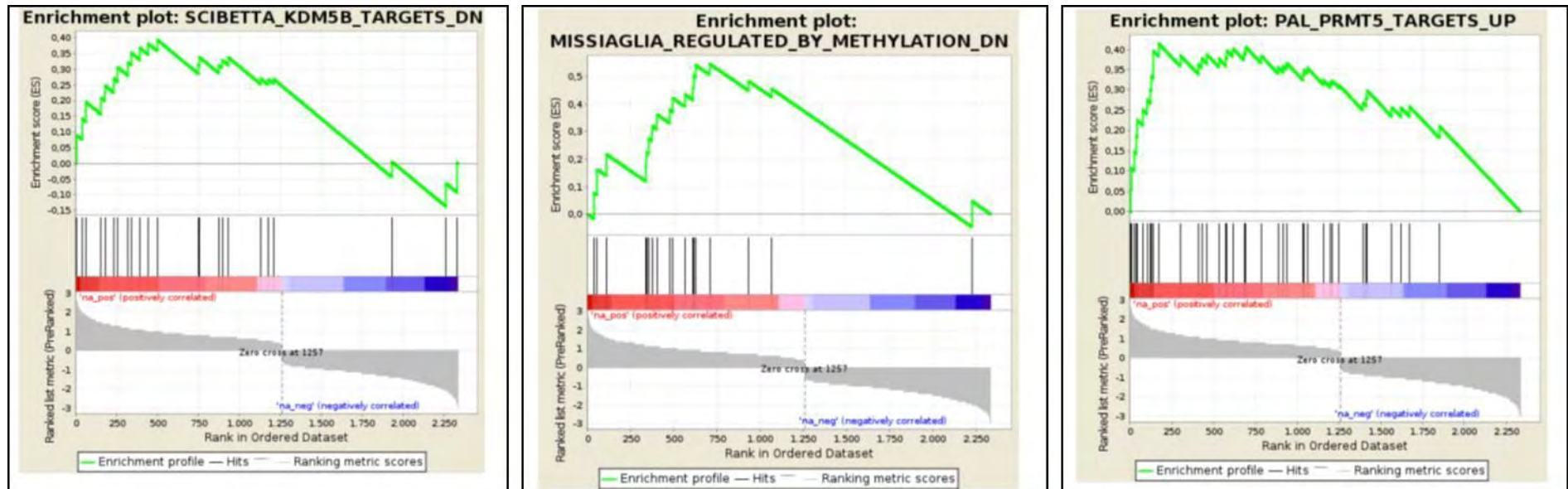
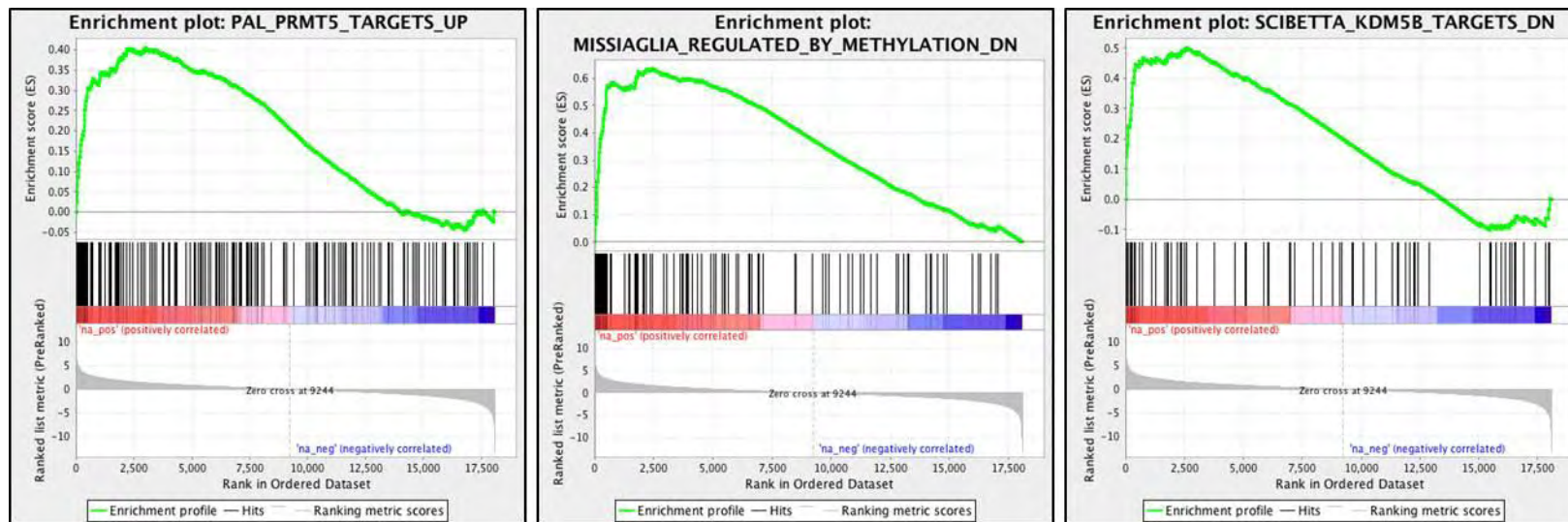


Figure S5. Gene Set Enrichment Analysis (GSEA) in CAL-1 cell line. Representative plots illustrate. in CAL-1 the enrichment of the same gene signatures recognized also in BPDCN samples: the *KDM5B* and *PRMT5* gene signatures reported in literature^{12,13} and also the enrichment of a set of genes. described by Missiaglia¹⁴ et al as responsive to a hypomethylating treatment. namely the Decitabine. NES normalized enrichment score ≥ 1.8 ; FDR q-val. false discovery rate ≤ 0.06



Supplemental References

1. Swerdlow SH, Campo E, Hazzis NL, et al. Facchetti F, Jones D, Petrella T. Blastic plasmacytoid dendritic cell neoplasm. In: Swerdlow SH, Campo E, Hazzis NL, et al., eds. WHO Classification of Tumors of Haematopoietic and Lymphoid Tissues. Lyon: IARC press; 2008:145-147.
2. Li H, Durbin R. Fast and accurate short read alignment with Burrows-Wheeler transform. *Bioinformatics*. 2009;25(14):1754-1760.
3. Trifonov V, Pasqualucci L, Tiacci E, Falini B, Rabadan R. SAVI: a statistical algorithm for variant frequency identification. *BMC Systems Biology*. 2013;7(Suppl 2):S2.
4. Wang J, Vasaikar S, Shi Z, Greer M, Zhang B. WebGestalt 2017: a more comprehensive, powerful, flexible and interactive gene set enrichment analysis toolkit. *Nucleic Acids Research*. 2017;45(W1):W130-W137.
5. Talevich E, Shain AH, Botton T, Bastian BC. CNVkit: Genome-Wide Copy Number Detection and Visualization from Targeted DNA Sequencing. *PLoS Comput Biol*. 2016; 21;12(4).
6. Dobin A, Davis C, Schlesinger F et al. STAR: ultrafast universal RNA-seq aligner. *Bioinformatics*. 2013;29(1):15-21.

7. Anders S, Huber W. Differential expression analysis for sequence count data. *Genome Biol.* 2010; 11:R106.
8. Subramanian A, Tamayo P, Mootha V, et al. Gene set enrichment analysis: A knowledge-based approach for interpreting genome-wide expression profiles. *Proceedings of the National Academy of Sciences.* 2005;102(43):15545-15550.
9. Fanelli M, Amatori S, Barozzi I, et al. Pathology tissue-chromatin immunoprecipitation, coupled with high-throughput sequencing, allows the epigenetic profiling of patient samples. *Proceedings of the National Academy of Sciences.* 2010;107(50):21535-21540
10. Ye T, Krebs A, Choukrallah M, et al. seqMINER: an integrated ChIP-seq data interpretation platform. *Nucleic Acids Research.* 2011;39(6):e35-e35.
11. Agliano A, Martin-Padura I, Marighetti P, et al. Therapeutic effect of lenalidomide in a novel xenograft mouse model of human blastic NK cell lymphoma/blastic plasmacytoid dendritic cell neoplasm. *Clinical Cancer Research.* 2011;17(19):6163-6173.
12. Scibetta AG, Santangelo S, Coleman J, et al. Functional analysis of the transcription repressor PLU-1/JARID1B. *Molecular and Cellular Biology.* 2007;27(20):7220-7235
13. Pal S, Vishwanath SN, Erdjument-Bromage H, Tempst P, Sif S. Human SWI/SNF-associated PRMT5 methylates histone H3 arginine 8 and negatively regulates expression of ST7 and NM23 tumor suppressor genes. *Molecular and Cellular Biology.* 2004;24(21):9630-9645.

14. Missiaglia E, Donadelli M, Palmieri M, Crnogorac-Jurcevic T, Scarpa A, Lemoine NR. Growth delay of human pancreatic cancer cells by methylase inhibitor 5-aza-2'-deoxycytidine treatment is associated with activation of the interferon signalling pathway. *Oncogene*. 2005;24(1):199-211